Potential diagenetic and detrital sources for calcareous sediments from the Carlsberg Ridge, Indian Ocean

Anil B. Valsangkar[1,*], D. V. Borole[1], Archana S. Shejwalkar[2], Niyati G. Kalangutkar[1], Nelita O. Fernandes[3] and Cliffa C. Dias[1]

[1]National Institute of Oceanography, Dona Paula, Goa 403 004, India
[2]Present address: School of Earth and Ocean Sciences, University of Victoria, Victoria BC, Canada
[3]Present address: Directorate of Mines and Geology, Panaji, Goa 403 001, India

Six sediment cores from the Carlsberg Ridge (CR) were studied for elemental concentration, magnetic susceptibility (χ), grain size and clay mineral distribution, and sedimentation rate to decipher possible detrital and diagenetic contributions. The sediments were characterized by very low χ, moderate total organic carbon, high $CaCO_3$ content and high accumulation rate (3 cm/ kyr). Clay mineralogical and geochemical data suggest major continental source from the Arabian Sea, and very low Mn distribution, absence of tephra and characteristic magnetic signatures rule out volcanic or hydrothermal input. Consistent peaks around 10, 25, 45, 60 and 80 cm depth and high uranium are due to sedimentary diagenesis.

Keywords: Diagenesis, elemental concentration, magnetic susceptibility, sedimentation rate.

THE Carlsberg Ridge (CR) in the Indian Ocean separates the Arabian Basin from the Somali Basin. The CR has a typical rough morphology with non-transform discontinuities similar to slow-spreading ridges like the northern portion of the Mid-Atlantic Ridge (MAR). Previous studies[1–5] on the CR have specified half-spreading rate varying between 1.2 and 1.5 cm/yr, and the sub-bottom profiler records indicate the presence of isolated sediment cover only in the NW part of the CR. Although some studies[6] have considered the possibility of hydrothermal activity along the CR to explain higher concentrations of Cu and Ni in the Arabian Sea sediments, there is no direct evidence. Unlike the Pacific and Atlantic Oceans[7,8], the CR sediments are not metalliferous, and are devoid of sulphide minerals.

In a recent cruise to the CR, an unusually large event plume was encountered[9,10], indicating sporadic volcanic and tectonic activity along the slow-spreading CR causing cataclysmic release of hydrothermal fluids. However, our attempts during the SK-207 cruise did not show such anomalous results[11] and suggested no hydrothermal input in the area. During surveys by the National Institute of Oceanography (NIO), ~120 km NW section of the CR was mapped using multi-beam bathymetry system, where upper mantle and lower crustal rocks were recovered[12]. Here we discuss the presence of diagenetic and detrital signatures in the sediments from the axial valley and flank regions of the CR using new geochemical, radiochemical, clay mineralogical and magnetic susceptibility data, and present the sedimentation rates.

Methodology

Sampling techniques

In a small portion out of the 440 km long section, a small segment of axial valley and flank region of NW CR in the Indian Ocean encloses thick sediments, from where six sediment cores were collected using spade and gravity corer (Figure 1) during SK-114 and SK-154 of *ORV Sagar Kanya* cruises. Spade core sediments (SPC-01 and

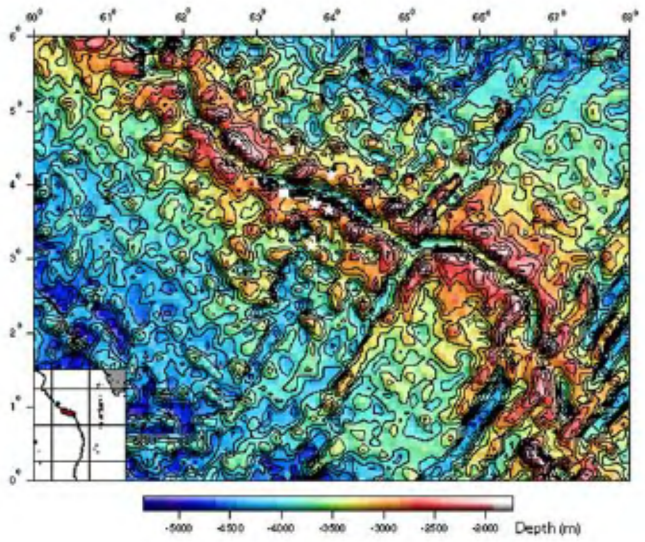

Figure 1. Sample locations in axial valley and flank region of Carlsberg Ridge with bathymetry contours. 1 = SPC-01, 2 = SPC-02, 3 = GC-03, 4 = GC-04, 5 = GC-05 and 6 = GC-06.

*For correspondence. (e-mail: vals@nio.org)

Table 1. ^{230}Th isotopes in SK-154, GC-04 core sediments

Depth (cm)	$CaCO_3$ %	^{238}U (dpm/g)	^{234}U (dpm/g)	^{232}Th (dpm/g)	^{230}Th (dpm/g)	$^{230}Th_{exc}$ (dpm/g)
0–2	32.3	0.39 ± 0.01	0.63 ± 0.01	0.46 ± 0.04	8.87 ± 0.37	8.24 ± 0.37
4–6	37.3	1.12 ± 0.02	1.52 ± 0.03	0.69 ± 0.06	11.04 ± 0.51	9.51 ± 0.51
30–32	49.0	0.51 ± 0.01	0.64 ± 0.01	0.63 ± 0.05	9.75 ± 0.33	9.11 ± 0.33
40–42	53.6	0.79 ± 0.01	1.09 ± 0.02	1.10 ± 0.10	12.57 ± 0.58	11.48 ± 0.58
55–60	24.2	1.98 ± 0.04	3.45 ± 0.07	0.37 ± 0.04	4.11 ± 0.21	0.67 ± 0.22
68–70	48.2	0.85 ± 0.02	0.82 ± 0.02	1.12 ± 0.11	9.19 ± 0.48	8.38 ± 0.48
95–100	38.6	0.80 ± 0.02	1.36 ± 0.03	1.04 ± 0.08	6.95 ± 0.29	5.59 ± 0.29
108–110	44.8	1.01 ± 0.02	1.47 ± 0.03	1.14 ± 0.07	7.19 ± 0.25	5.72 ± 0.26
120–125	43.9	1.22 ± 0.02	0.76 ± 0.01	1.53 ± 0.14	7.55 ± 0.39	6.79 ± 0.39
122–125	42.6	0.75 ± 0.01	1.05 ± 0.02	1.20 ± 0.14	7.28 ± 0.47	6.23 ± 0.47

0.75 dpm = 1 ppm for ^{238}U; 0.242 dpm = 1 ppm for ^{232}Th.

SPC-02) of SK-114 were sub-sectioned @ 2 cm interval up to 10 cm and then @ 5 cm up to the end, whereas four gravity cores (GC-03, GC-04, GC-05 and GC-06) from SK-154 were sub-sectioned @ 2 cm interval from top to the end of the core.

Grain size and clay mineralogy

Sediment texture was determined by the standard pipette analysis[13] and oriented slides of 2 μm size clay fractions were made using 1 ml of treated sample for X-ray diffraction measurements carried out on Philips X-ray diffractometer (PW 1840) with Ni-filtered CuKα radiation, from 3° to 22° 2θ/min, operated at 20 mA and 40 kV. Percentage of clay minerals was determined by weighted peak area method[14]. Total organic carbon (TOC) was estimated by following the wet oxidation method[15] with dichromate. $CaCO_3$ % was determined using CO_2 Coulometer of UIC Inc., Model 5014. For this purpose, about 15–20 mg of the sample was used to acidify with 1 N HCl solution to liberate CO_2. The accuracy was <0.1% and the precision was better than ± 5%.

Chemical composition

Transition metal concentration of Fe and Mn by XRF, and Si and Al by ICP-MS was determined at NGRI, Hyderabad. For precision and accuracy of the analysis, six internal and international standards (JP-1, NIM-P, JB-3, GSR-3, JSB-1 and JB-2) were included. To determine magnetic susceptibility (χ), sediment samples were filled in non-magnetic, plastic sample holders of 8 cc capacity and oven-dried at 40°C. Low-frequency mass-specific magnetic susceptibility (χ) of the samples was measured on a Bartington magnetic susceptibility meter (model MS2). After switching on the instrument, it was allowed to warm up for half an hour. The mass-specific magnetic susceptibility (χ_{lf}, 10^{-8} m^3 kg^{-1}) was calculated from the data obtained with the MS2 meter.

Radiochemical measurements

Uranium–thorium (U–Th) radiochemical separation and purification were carried out following the standard procedure[16], and ^{232}Th decay method was employed for determination of sedimentation rates (Table 1). The ^{230}Th excess (i.e. portion of ^{230}Th not supported by the decay of ^{234}U in the sediments) was calculated by subtracting the ^{234}U from the total ^{230}Th activity, using the equation: $^{230}Th_{exc}$ (dpm/g) = ^{230}Th (dpm/g) – ^{234}U (dpm/g).

Results

The present study includes various results on the sub-sections up to 100 cm depth. Elemental results are presented here on carbonate free basis (cfb), unless, otherwise mentioned.

Axial valley sediments

Totally three cores were obtained from the axial valley during SK-114 (SPC-01) and SK-154 (GC-03 and GC-04) cruise. The relative abundance of clay minerals in SPC-01 sediments (clayey-silt) indicated that illite (23–40%) and chlorite (22–46%) were the most dominant minerals than smectite (6–38%) and kaolinite (13–20%). Smectite was the highest only in the top surface; otherwise, it was the lowest among others (Figure 2 *a*). Illite, kaolinite, clay (Figure 2 *a*), TOC and carbonate (Figure 3 *a*) displayed higher value peak at 8–10 cm depth. Sand (8–12%) decreased and clay (31–46%) increased with depth (Figure 2 *a*). Fe and Mn content also increased from 20 cm depth (Figure 3 *a*).

The GC-03 core sediments behaved similarly, where $CaCO_3$, TOC and illite increased with depth, and sand (7–3%), and smectite (39–4%) showed a decrease. Kaolinite and chlorite displayed large variation and mixed behaviour. Noticeable changes occurred at 50 to 54 cm depth, where smectite, kaolinite, chlorite, sand, clay and Mn

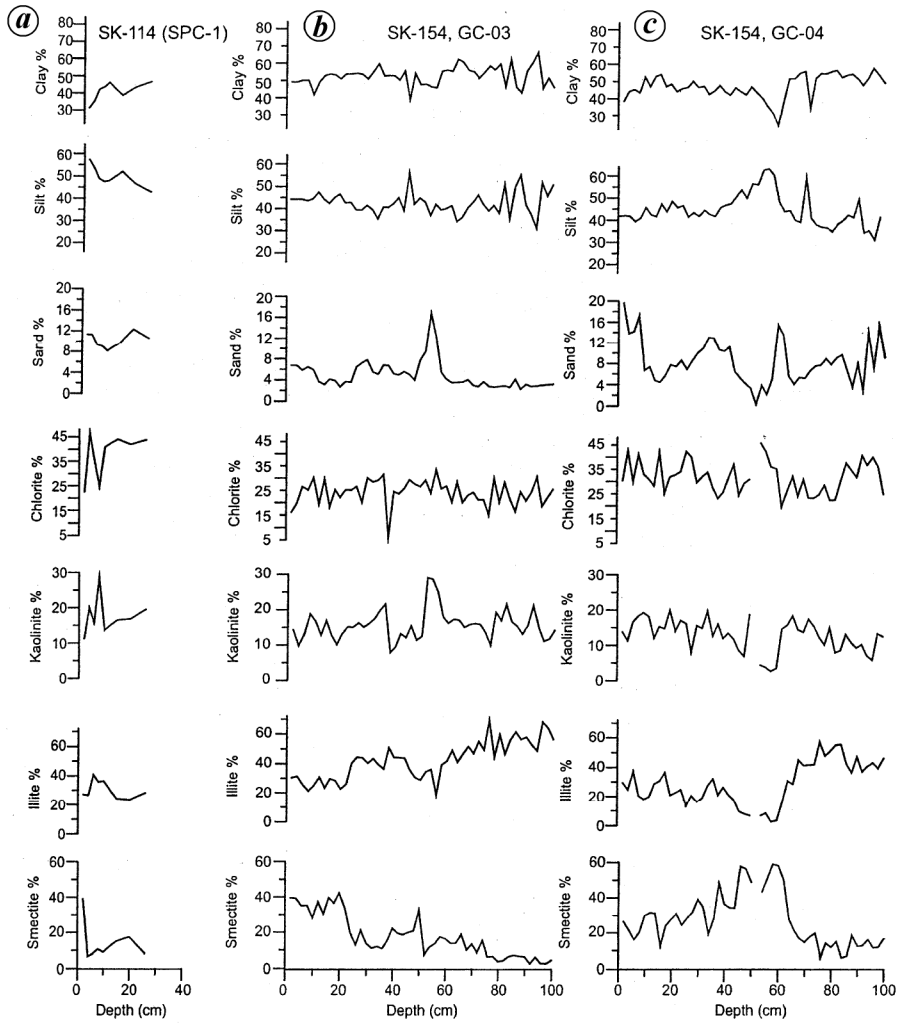

Figure 2 *a–c*. Profiles of clay minerals and sand–silt–clay content for SPC-01, GC-03 and GC-04 respectively.

were higher (Figure 2 *b*) and $CaCO_3$, TOC, Fe and susceptibility showed lower values (Figure 3 *b*). Fe was higher at the surface (7.3%) and varied little with depth, and had small peaks at 26 and 42 cm depth (Figure 3 *b*). Mn showed small increase from the surface to 48 cm depth, with small peaks at 24 and 46 cm, and then decreased to 0.06%. Susceptibility also showed small increase with depth (0.3–1.2 X_{lf}) and a break from 46 cm depth (Figure 3 *b*). TOC was the highest (0.51%) at 80 cm depth.

The olive grey sediments of GC-04 exhibited distinct changes at 55–60 cm depth. Up to 50 cm depth, there was overall decrease in sand, illite, kaolinite and chlorite, and increase in clay and smectite content (Figure 2 *c*). Carbonates declined sharply (53–14%) from 40 to 60 cm depth, where Mn, Fe and TOC had higher peak value, indicating lithological changes (Figure 3 *c*). TOC and Fe values were constant up to 44 and 48 cm depth respectively, and then increased (Figure 3 *c*). Mn displayed a peak at 10 and 50 cm depth. The silty-clay sediments had comparatively higher susceptibility value at the surface (1.6), which decreased down core to 0.36 X_{lf} with a change at 48–50 cm depth.

Flank sediments

Flank sediments include two cores from the north (SPC-02 and GC-05) and one from the south (GC-06). Illite and chlorite dominated the silty-clay sediments of SPC-02. The down-core profiles showed decrease in smectite, kaolinite, sand and silt content and increase in illite, chlorite and clay proportions (Figure 4 *a*). Similarly, carbonates and Fe showed an increase, while Mn (0.6–0.1%) and TOC (0.3–0.1%) decreased (Figure 5 *a*). Fe had a large range compared to Mn.

Silty-clay sediments of GC-05 exhibited similar down-core trends, where illite, chlorite and clay showed an increase, while smectite, kaolinite and sand decreased (Figure 4 *b*). Fe had a wide range and decreased with depth up to 2%. Mn had a small peak around 22–40 cm, where Fe was

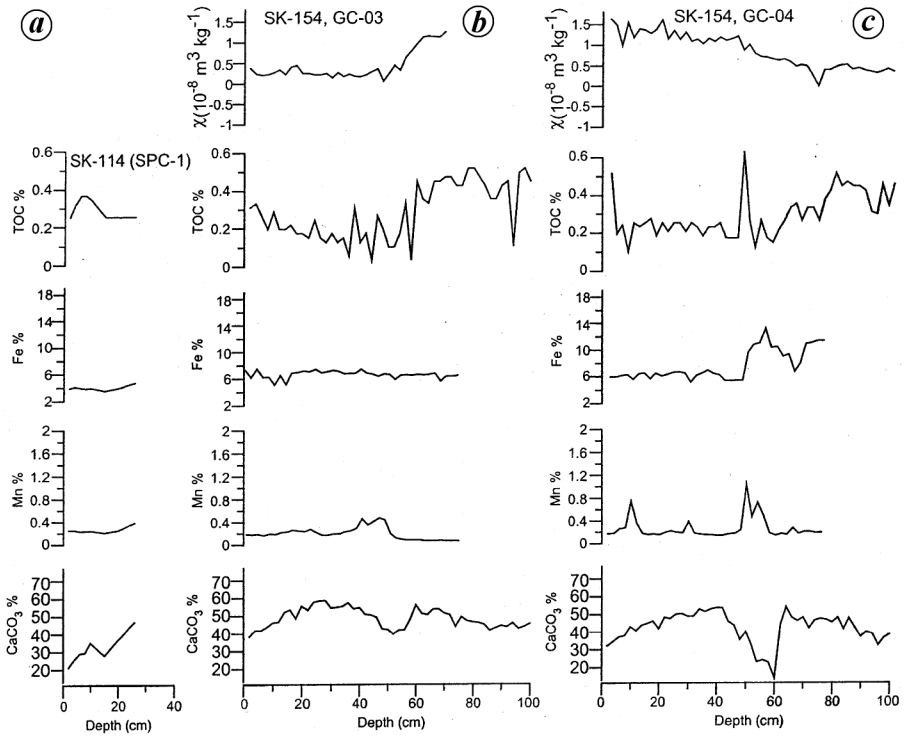

Figure 3 *a–c.* Profiles of carbonate, Mn, Fe, total organic carbon (TOC) and magnetic susceptibility (χ) for SPC-01, GC-03 and GC-04 respectively.

comparatively lower. Noticeable changes in carbonate, Mn, Fe and TOC content were marked from 50 to 60 cm depth (Figure 5 *b*). TOC was noticeably high (0.4%) at 52 cm and magnetic susceptibility (MS) was maximum (0.37 X_{lf}) at 48 cm depth.

GC-06 core sediments (SW flank) were silty-clay, where illite and clay showed a gradual increase, and others showed a down-core decrease (Figure 4 *c*). MS decreased with increase in Fe with depth (Figure 5 *c*). Higher Mn occurred for 36–56 cm sections, but noticeable changes were seen from 75 to 80 cm depth, where Fe, Mn and TOC content increased and $CaCO_3$ dropped to 48%. Similarly, higher peak value for carbonate and Mn, and lower peak value of Fe and TOC occurred at ~60 cm depth (Figure 5 *c*).

All the cores had similar down-core trends for Si and Al (Figures 6 and 7 respectively), with peaks at around 6, 10, 14, 26, 33, 52 and 80 cm. Similarly, Mn/Al ratio had higher peak values at different depths (Figure 8). In most cores, the Mn/Al peak was seen around 40 cm depth. Variation in K content for axial valley sediment (1.3–3.9%) was comparatively smaller than that for the flank sediments (0.8–8.0%). Except for GC-05, the down-core profiles of all other cores showed an increase of K with depth (Figure 9).

U–Th dating

The decay curve up to 125 cm depth (excluding the 55 cm plot) appears to be linear (Figure 10). The estimated sediment accumulation rate from $^{230}Th_{ex}$ decay profile for GC-04 core works out to be 3.03 ± 0.14 cm/kyr (n = 11; r = –0.6 and $P \leq 0.05$) for the top to 125 cm down core (11 samples, excluding the one at 55 cm). With this rate, the base of the core at 100 cm depth was estimated to be 33 kyr old.

Discussion

Source of CR sediments

Terrigenous source: The CR sediments are silty-clay throughout, except for the top 50–60 cm in the axial valley, where presence of both silty-clay and clayey-clay indicates mixing of the sediments (Table 2). Despite differential inputs, the Si and Al down-core profiles (Figures 6 and 7 respectively) are analogous and strongly imply a single (terrigenous) source for the CR sediments. The flank sediments of the CR are characterized by high illite (40–50%) and low smectite (< 20%), whereas the axial valley sediments have comparatively low illite (30–40%) and high smectite clay (30–40%). Illite is most abundant clay mineral in the Indus River sediments and in the Iran-Makran soils[17]. Illite is also the dominant clay mineral in the northern Arabian Sea sediments, which has the highest concentrations in sediments in the areas between the Indus Fan and the Persian Gulf[18]. The ODP site 728 A in the NW Arabian Sea also has illite and chlorite as the most dominant clay minerals influenced by the terri-

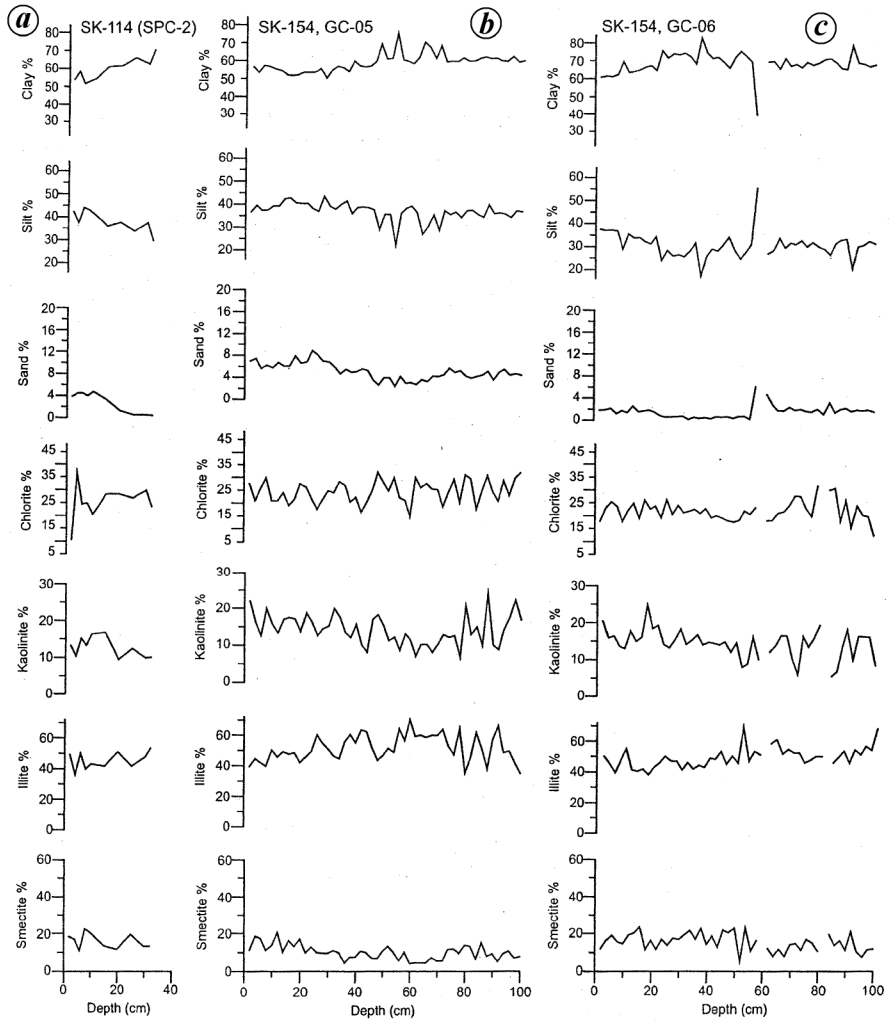

Figure 4 *a–c*. Profiles of clay minerals and sand–silt–clay content for SPC-02, GC-05 and GC-06 respectively.

genous fractions[19]. The northwesterly wind system which was dominant during the Holocene, appears to be responsible for sediment transportation to the Arabian Sea[20]. Therefore, high illite and chlorite (~20–30% in the axial valley and ~18–35% on the flanks) in the CR sediments strongly points towards Arabian Sea source, which in turn has a mixed source, predominantly from the Indus.

The supply of smectite clay to the Arabian Sea sediments from the Bay of Bengal[21] or far from the southern latitudes below the equator due to melting of ice has been doubted by previous workers[22]. The Indus River originates in Tibet and follows the Indus Suture Zone through the Dras volcanics (island arc basalts and dacites) in the Himalayan mountain ranges and arid regions of Pakistan–India and drains to the Arabian Sea. The major source of smectite to the eastern Arabian Sea is from the Deccan Trap, whereas the Arabian Peninsula, Persian Gulf and Gulf of Oman have minor contribution of smectite in the western Arabian Sea[19]. The smectite abundance from 25°N to 5°N (close to the CR) in the Arabian Sea has been reported[17] to be constant or <20%. It is reported that the high smectite band (>40–50%) exist around 20°N in the Arabian Sea is due to dispersion of smectite by the Narmada and Tapti rivers towards west by the westward and northward currents and oceanic circulation[17], and that the smectite from the rivers is not transported towards south as revealed from the decrease in smectite content (<10%) along the South Indian margin[17]. Therefore, it is opined that smectite (10–20% on the flanks) in the CR sediments is derived from the Arabian Sea (similar to illite) and not from the Indian margin. However, presence of high smectite (30–40%) in the axial valley further point towards an additional source, which appears remote due to the alteration of volcanic basalts in the absence of volcanic or hydrothermal activity in the CR. Therefore, the source of smectite for the axial valley sediments is the most likely from the African soil, brought to the CR by the northerly-bound equatorial currents, and the arid source[19] is doubtful due to low crystallinity of the smectite clay.

The observed increase in K content with depth in almost all the sediment cores from the axial valley and flank

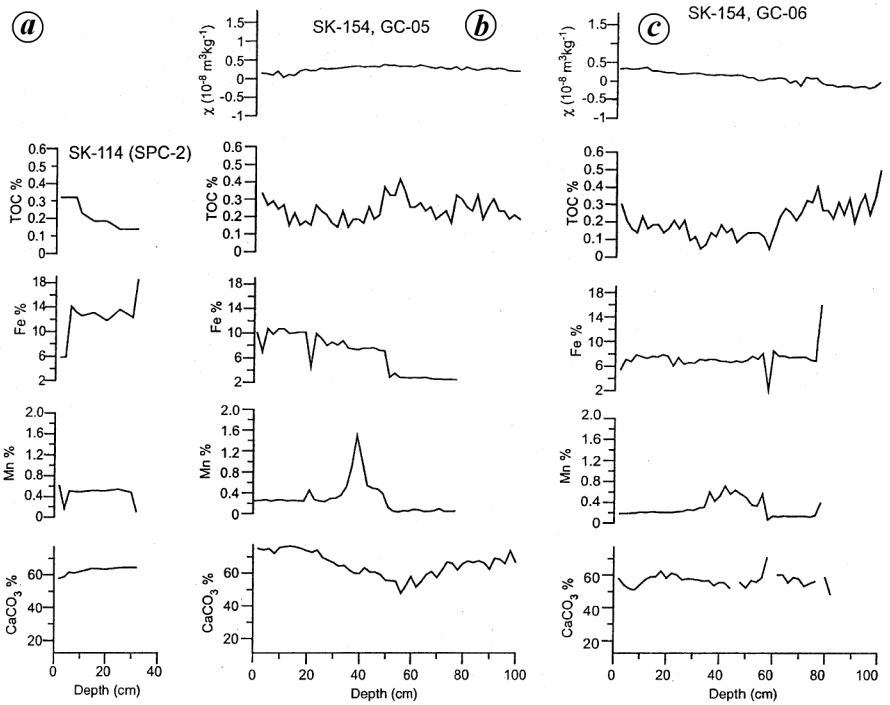

Figure 5 *a–c*. Profiles of carbonate, Mn, Fe, TOC and MS (χ) for SPC-02, GC-05 and GC-06 respectively.

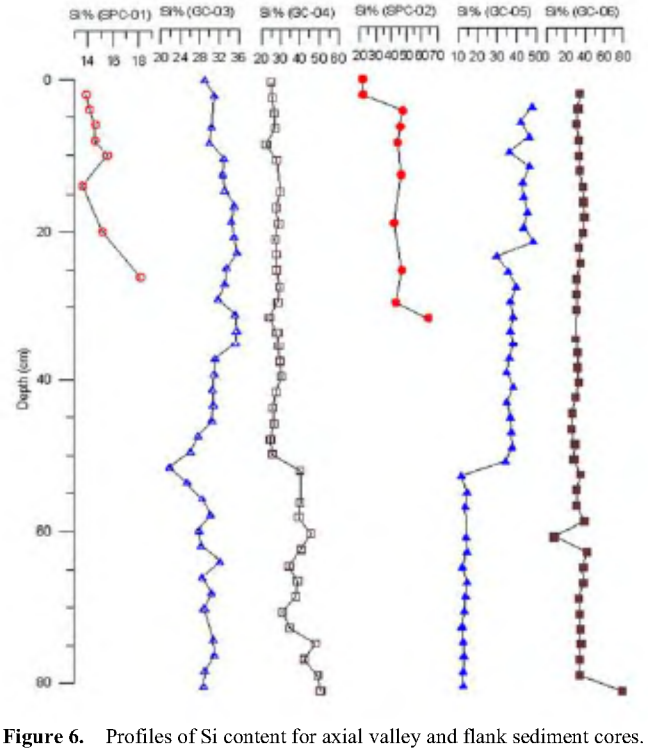

Figure 6. Profiles of Si content for axial valley and flank sediment cores.

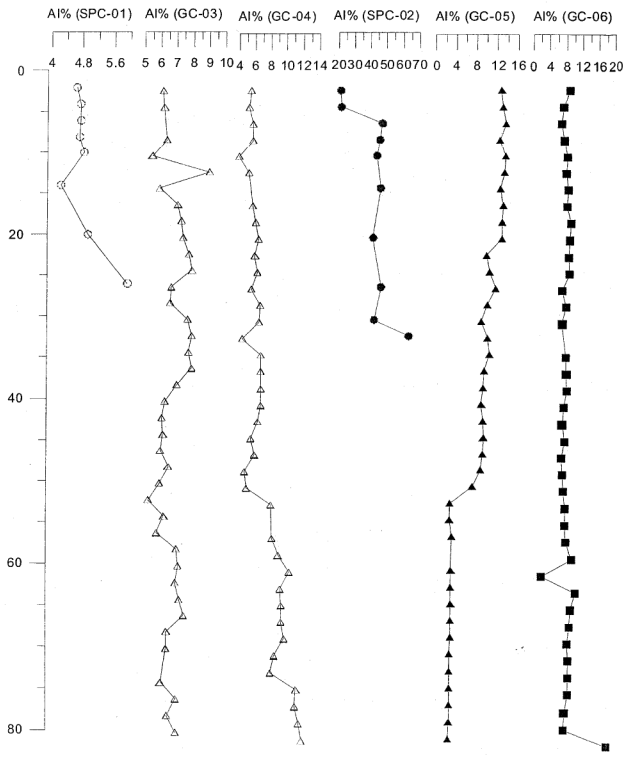

Figure 7. Profiles of Al content for axial valley and flank sediment cores.

regions (Figure 9) suggests the larger detrital input for the deeper samples. Relatively high kaolinite (12–15% in the valley and 13–22% on flanks) is probably derived from the tropical soils of southern India and Africa–Madagascar due to northerly-bound equatorial circulation currents from south of the CR, as suggested earlier[17].

Biogenic source

TOC variation in the sediments (0.3–0.5%) is normal and within the range of deep-sea sediments. The flank sedi-

ment cores were retrieved between 3700 and 4600 m water depths. The higher $CaCO_3$ (47–76%) in the flank sediments suggests no effect of dissolution of $CaCO_3$ and indicates deeper lysocline depth. The sediment cores from depth range 4300–4400 m in the axial valley have comparatively lower carbonates (17–58%), which shows an increase with depth (Figures 3 *a–c*) and supports deeper lysocline in the CR. The CR crest is known for high biological productivity and samples have high foraminiferal abundance. Higher carbonate content (>70%) in the flank sediments also indicates higher sedimentation rates in the area, and that high biological productivity and high sedimentation rates are responsible for high carbonate flux in the CR area, which is also acting as a strong diluent on the other elemental phase, as observed earlier[23].

Volcanic source

Magnetic fractions in sediments are normally derived from volcanic and terrigenous inputs, biogenic minerals and diagenetic alteration[24]. Absence of tephra material (volcanic) in sand-sized fractions of the CR sediments clearly indicates absence of volcanic activity in the area. Absence of distinct susceptibility peaks in the down-core profiles of all the sediment cores further suggests no volcanic or hydrothermal contribution from any nearby source. Both these indicators imply that the sediment source for the CR is non-volcanic.

Hydrothermal signatures

Enrichment of Mn is considered as one of the important hydrothermal signatures, as Mn could be incorporated either by diagenitic or hydrothermal source. Mn profiles for all the cores showed no significant enrichment in the top sediments (Figures 3 and 5), which behaved as normal pelagic sediments[25]. Sharp peaks of Mn observed at different depths in all the cores appeared to be typical of oxidation fronts in diagenetic system[26–28] and suggest that higher Mn may not be due to hydrothermal input and that diagenetic processes play a key role. Although Mn variation was low to moderate (0.06–1%) for valley sediments, the overall range was up to 0.5% and spikes of 0.7 and 1% were observed at a few depths (8–10, 50–52 and 56–58 cm, Figure 3 *c*) in GC-04 core sediments. Although Mn ranged from very low to moderately high values for flank sediments (0.03–1.5%), the actual range remained up to 0.6%, leaving spikes of >1% at 38 to 42 cm depth in

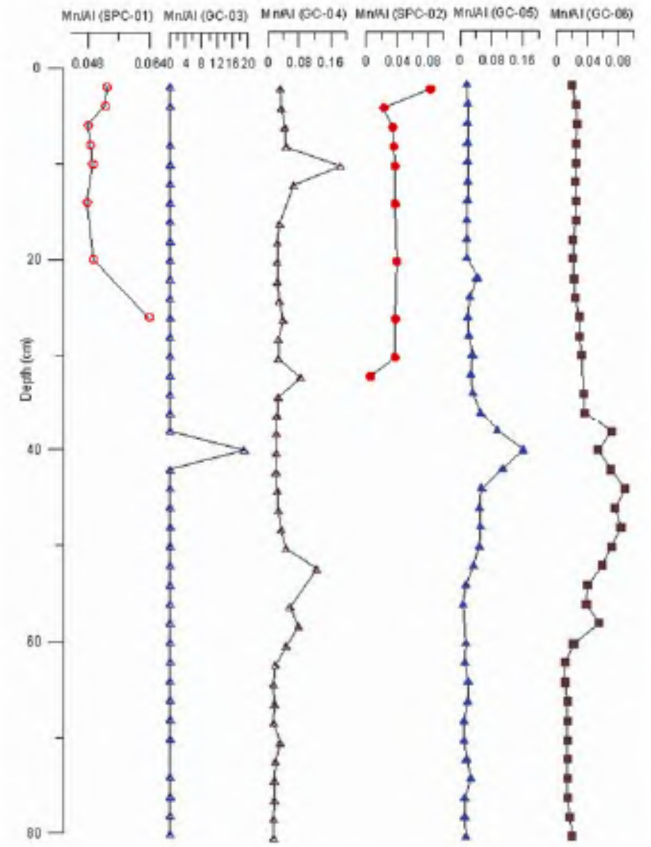

Figure 8. Profiles of Mn/Al ratio for axial valley and flank sediments.

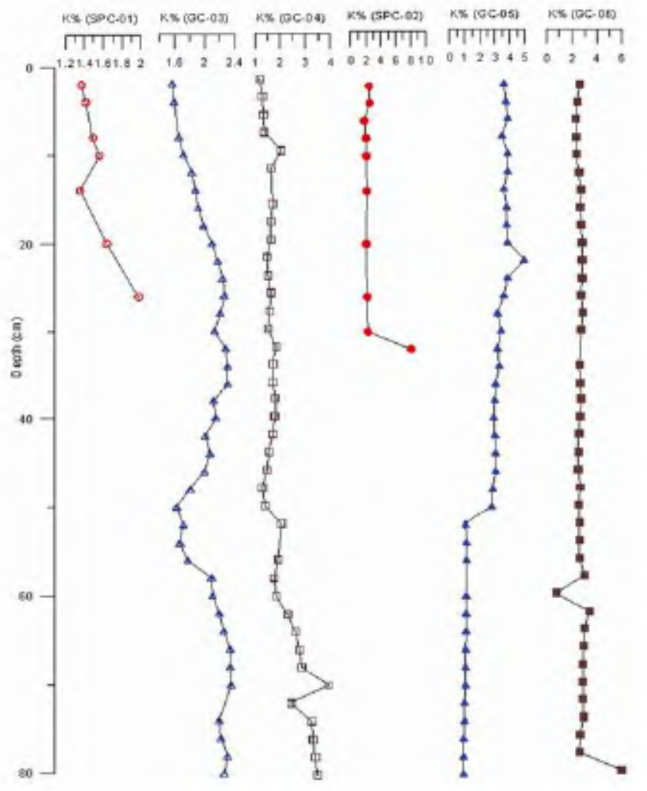

Figure 9. Profiles of K content for axial valley and flank sediments.

Table 2. Sediment texture and major clay minerals from Carlsberg Ridge

Location	Sample no.	Core depth (cm)	Sediment type	Major type sediment	Decreasing abundance of clay minerals
Axial valley	SK-114, SPC-1	0–20	Clayey-silt	Clayey-silt	0–2: SIKC
		20–26	Silty-clay		2–4: CIKS
					4–8: ICKS
					8–26: CIKS
Axial valley	SK-154, GC-03	0–44	Silty-clay	Clayey-silt and	0–22: SICK
		44–46	Clayey-silt	Silty-clay	22–36: ICKS
		45–80	Silty-clay		36–50: ICSK
		80–82	Clayey-silt		50–100: ICKS
		82–86	Silty-clay		
		86–88	Clayey-silt		
		88–94	Silty-clay		
		94–96	Clayey-silt		
		96–98	Silty-clay		
		98–100	Clayey-silt		
Axial valley	SK-154, GC-04	0–2	Clayey-silt	0–38: Silty-clay	0–8: CISK
		2–16	Silty-clay	38–62: Clayey-silt	8–28: CSIK
		16–18	Clayey-silt	62–100: Silty-clay	28–62: SCIK
		18–20	Silty-clay		62–100: ICSK
		20–22	Clayey-silt		
		22–32	Silty-clay		
		32–34	Clayey-silt		
		34–38	Silty-clay		
		38–62	Clayey-silt		
		62–70	Silty-clay		
		70–72	Clayey-silt		
		72–90	Silty-clay		
		90–92	Clayey-silt		
		92–100	Silty-clay		
NW flank	SK-114, SPC-2	0–32	Silty-clay	Silty-clay	0–32: ICSK
NW flank	SK-154, GC-05	0–100	Silty-clay	Silty-clay	0–100: ICKS
SW flank	SK-154, GC-06	0–56	Silty-clay	Silty-clay	0-100: ICSK
		56–58	Clayey-silt		
		58–60	No sample		
		60–100	Silty-clay		

S, Smectite; I, Illite; K, Kaolinite and C, chlorite.

Table 3. Inter-element relationship of axial valley sediments

	SPC-01; $N = 8$			GC-03; $N = 35$				GC-04; $N = 38$			
	Fe	Mn	TOC	Fe	Mn	TOC	MS	Fe	Mn	TOC	MS
Depth	0.45	0.62	–0.43	–0.08	–0.22	0.29	0.69	0.72	0.01	0.16	–0.90
Fe		0.95	0.47		0.23	–0.23	–0.25		0.26	0.02	0.75
Mn			0.58			0.25	–0.65			0.04	0.05
TOC			1.00				0.67				0.20
	$r = 0.67$, CL = 95%			$r = 0.33$, CL = 95%				$r = 0.32$, CL = 95%			

r = Correlation coefficient; CL = Confidence level.

GC-05 and 0.7% at 42–44 cm depth in GC-06 (Figure 5 *b* and *c* respectively). The ternary diagrams[29] show that the field occupied by the CR plots is close to that of the Pacific sediments (Figures 11 and 12) and strongly rule out the possibility of hydrothermal activity, which could be a possible cause for the Mn enrichment.

Diagenetic signatures

The CR sediments have dissimilar down-core MS profiles compared to Fe and Mn content (Figures 3 *b*, *c* and 5 *b*, *c*), and inverse relationship between TOC and $CaCO_3$ (Figures 3 *a–c* and 5 *a–c*) suggesting diagenetic influence. In the absence of hydrothermal input in the CR, the observed strong correlation of Fe and Mn in SPC-01 (0.95, Table 3), or significant correlation in GC-05 (0.35, Table 4), and the sudden increase in Fe and Mn at ~ 26 cm depth in SPC-01 (Figure 3 *a*), at 45 cm depth in GC-04 (Figure 3 *c*), and at 80 cm depth in GC-06 (Figure 5 *c*) is possible due to strong diagenetic influence in the sediments. Most Mn peaks occurring at different depths in the CR sediments were sharp, which is typical of

Table 4. Inter-element relationship of flank sediments

	SPC-02; $N = 10$			GC-05; $N = 39$				GC-06; $N = 39$			
	Fe	Mn	TOC	Fe	Mn	TOC	MS	Fe	Mn	TOC	MS
Depth	0.68	–0.25	–0.95	–0.89	–0.27	0.21	0.67	0.24	0.02	0.33	–0.91
Fe		–0.19	–0.58		0.39	0.35	0.56		0.11	0.26	0.15
Mn			0.18			–0.26	0.11			– 0.43	–0.03
TOC			1.00				0.14				0.18
	$r = 0.58$, CL = 95%			$r = 0.31$, CL = 95%				$r = 0.32$, CL = 95%.			

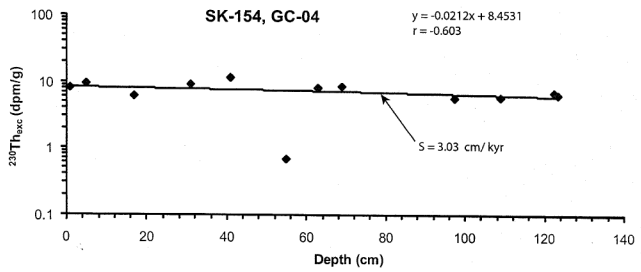

Figure 10. ^{230}Th ex profile for GC-04 sediment core showing sedimentation rate = 3.03 cm/kyr (excluding plot ~58 cm). Correlation (–0.6) is above the level of significance (0.55 for $n = 11$).

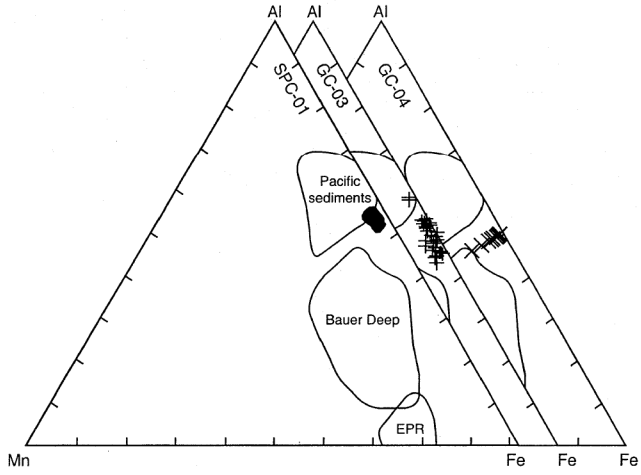

Figure 11. Ternary diagram of Al, Fe and Mn for axial valley sediment cores (SPC-01, GC-03 and GC-04). EPR, East Pacific Rise.

migration of oxidation front in a diagenetic system[28]. Changes in Mn concentration of the sediments containing little organic matter is possible due to penetration of oxygen at depths[30]. The CR sediments contained a small quantity (< 0.6%) of TOC, and the down-core profiles for axial valley sediments showed an increase in Mn and decrease of TOC at about 15 cm depth in SPC-1 (Figure 3 *a*), indicating consumption of oxygen due to diagenesis. Similar inverse relation for Mn and TOC of GC-03 was observed at ~ 40 cm depth (Figure 3 *b*), and ~ 10 and 26 cm depth of GC-04 (Figure 3 *c*). However, increase in TOC, Mn and Fe at ~ 45 cm depth of GC-04 (Figure 3 *c*) may reflect oscillation of oxic–anoxic boundary layer due to pulsed sedimentation. The down-core profiles for flank

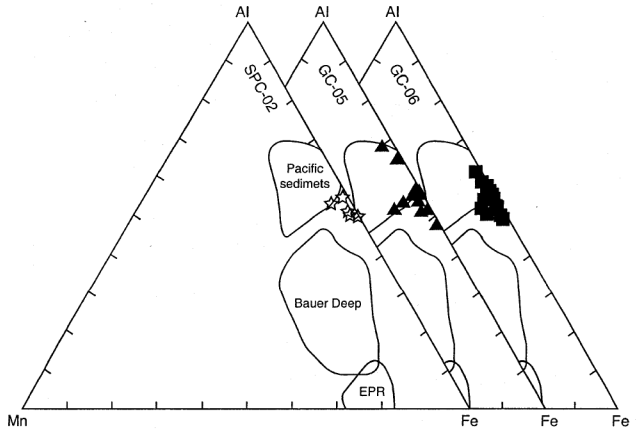

Figure 12. Ternary diagram of Al, Fe and Mn for sediment cores from flanks (SPC-02, GC-05 and GC-06).

sediments also showed an inverse relation of TOC and Mn in the surface sediments of SPC-2 (Figure 5 *a*), and displayed lower TOC value (< 0.2%) for peak value of Mn (1.6%) at ~ 40 cm depth of GC-05 (Figure 5 *b*) and GC-06 (Figure 5 *c*). However, as observed for the axial valley, the increase in TOC, Mn and Fe at ~ 85 cm depth in GC-06 (Figure 5 *c*) for the flank sediments is due to non-diagenetic effects.

Possibility of winnowing of high U in samples representing jumps of TOC, Mn (Figures 3 *a–c* and 5 *a–c*) and sand (Figures 2 *a–c* and 4 *a–c*), particularly around 50 cm depth has been ruled out as ^{230}Th depth profile (Figure 10) showed no winnowing except for the one low ^{230}Th excess at 55 cm depth. Therefore, high U in the analysed samples indicates diagenetic mobilization of U and that the internal sedimentary diagenesis has given rise to consistent peaks at around 10, 25, 45, 60 and 80 cm depth.

Conclusion

Clay mineralogical, geochemical and U–Th isotopic studies of sediments from the CR showed that the major sediment sources are continental, biogenic and diagenetic. The illite-rich sediments had high accumulation rates (3 cm/kyr) and were typically characterized by low Mn, very low χ, moderate TOC and high carbonate content. Absence of Mn enrichment, very low MS and monotonous down-core profile in all the cores rule out volcanic

or hydrothermal contribution in the sampling area. The ^{230}Th depth profile showed no winnowing, and internal sedimentary diagenesis appeared responsible for U enrichment and consistent peaks at different depths.

1. Le Pichon, X. and Heirtzler, J. R., Magnetic anomalies in the Indian Ocean and sea-floor spreading. *J. Geophys. Res.*, 1968, **73**, 2101–2117.
2. McKenzie, D. P. and Slater, J. G., The evolution of the Indian Ocean since the Late Cretaceous. *Geophys. J. R. Astron. Soc.*, 1971, **25**, 437–528.
3. Ramana, V., Ramprasad, T., Kamesh Raju, K. A. and Desa, M., Geophysical studies over a segment of a Carlsberg Ridge, Indian Ocean. *Mar. Geol.*, 1993, **115**, 21–28.
4. Chaubey, A. K., Bhattacharya, G. C., Murty, G. P. S. and Desa, M., Spreading history of the Arabian Sea: some new constraints. *Mar. Geol.*, 1993, **112**, 343–352.
5. Kamesh Raju, K. A., Kodagali, V. N. and Fujimoto, H., In Proceedings of 35th Annual Convention of Indian Geophysical Union, National Institute of Oceanography, Goa, 1998, pp. 29–30.
6. Shankar, R., Subbarao, K. V. and Kolla, V., Geochemistry of surface sediments from the Arabian Sea. *Mar. Geol.*, 1987, **76**, 253–279.
7. Rona, P. A., Black smokers and massive sulfides at the TAG hydrothermal field, Mid-Atlantic Ridge 26°N (abs.). *EOS*, 1985, **66**, 936.
8. Minniti, M. and Bonavia, F. F., Copper-ore grade hydrothermal mineralization discovered in a seamount in the Tyrrhenian Sea (Mediterranean): is the mineralization related to porphyry-coppers or to base metal lodes? *Mar. Geol.*, 1984, **59**, 271–282.
9. Murton, B. J., Baker, E. T., Sands, C. M. and German, C. R., Detection of an unusually large hydrothermal event plume above the slow-spreading Carlsberg Ridge, NW Indian Ocean. *Geophys. Res. Lett.*, 2006, **33**, 1–5.
10. Anon., Cruise report of *RSS Charles Darwin* (CD-149) (18 July–6 August 2003), Southampton Oceanography Centre, UK, p. 3.
11. Anon, Cruise report of *ORV Sagar Kanya* (SK-207) (13 July–19 August 2004), National Institute of Oceanography, Dona Paula, Goa, p. 27.
12. Mudholkar, A. V., Kodagali, V. N., Kamesh Raju, K. A., Valsangkar, A. B., Ranade, G. H. and Ambre, N. V., Geomorphological and petrological observations along a segment of slow-spreading Carlsberg Ridge. *Curr. Sci.*, 2002, **8**, 982–989.
13. Folk, R. L., *Petrology of Sedimentary Rocks*. Hemphills, Austin, 1968, p. 177.
14. Byscaye, P. E., Mineralogy and sedimentation of recent deep sea clay in Atlantic Ocean and adjacent seas and oceans. *Geol. Soc. Am. Bull.*, 1965, **76**, 803–831.
15. El Wakeel and Riley, J. P., Determination of organic carbon in the marine muds. *J. Cons. Perm. Int. Explor. Mer.*, 1957, **22**, 180–183.
16. Krishnaswami, S. and Sarin, M. M., The simultaneous determination of Th, Pu, Ra isotopes ^{210}Pb, ^{55}Fe; ^{32}Si and ^{14}C in marine suspended phases. *Anal. Chim. Acta*, 1976, **83**, 171–181.
17. Kolla, V., Kostecki, J. A., Robinson, F., Biscaye, P. E. and Ray, P. K., Distributions and origins of clay minerals and quartz in surface sediments of the Arabian Sea. *J. Sediment. Petrol.*, 1981, **51**, 563–569.
18. Goldberg, E. D. and Griffin, J. J., The sediments of the northern Indian Ocean. *Deep Sea Res.*, 1970, **17**, 513–537.
19. Das, S. S., Maurya, A. S., Pandey, A. C., Bhan, U. and Rai, A. K., Influence of sediment source and monsoonal variations on the late Quarternary clay mineral assemblages at ODP site 728A, northwestern Arabian Sea. *Curr. Sci.*, 2008, **95**, 1320–1326.
20. Sirocko, F. and Sarnthein, M., Wind-borne deposits in the northwestern Indian Ocean: Record of Holocene sediments versus modern satellite data. In *Palaeoclimatology and Palaeometeorology: Modern and Past Patterns of Global Atmospheric Transport* (eds Leinen, M. and Sarnthein, M.), NATO ASI Series, 1989, vol. 282, pp. 401–433.
21. Nigam, R., Borole, D. V. and Hashimi, N. H., Study of subsurface sediments from northern Indian Ocean: oceanic responses to climatic changes. *J. Palaeontol. Soc. India*, 1994, **39**, 1–4.
22. Hays, J. D., Lozano, J. A., Shackleton, N. J. and Irving, G., An 18000 BP reconstruction of the Atlantic and western Indian sectors of the Antarctic Ocean. In *Investigations of Late Quaternary Paleo-oceanography and Paleo-climatology* (eds Cline, R. M. and Hays, J. D.), Geological Society of America, Memoirs, 1976, vol. 145, pp. 337–374.
23. Valsangkar, A. B., Kaisiddaiah, S. M. and Ambre, N. V., Geochemistry, factor analysis and clay mineral distribution of the sediments and relationship with the associated ferromanganese nodules from the SW Carlsberg Ridge. *Mahasagar*, 1992, **25**, 83–95.
24. Roberts, A. P. and Turner, G. M., Diagenetic formation of ferrimagnetic iron sulphide minerals in rapidly deposited marine sediments, New Zealand. *Earth Planet. Sci. Lett.*, 1993, **115**, 257–273.
25. Rutten, A. and De Lange, G. J., Sequential extraction of iron, manganese and related elements in S1 sapropel sediment, eastern Mediterranean. *Palaeogeogr., Palaeoclimatol., Palaeoecol.*, 2003, **190**, 79–101.
26. Froelich, P. N., Klinkhammer, G. P., Bender, M. L., Luedtke, N. A., Heath, G. R., Cullen, D. and Dauphin, P., Early oxidation of organic matter in pelagic sediments of the eastern equatorial Atlantic: suboxic diagenesis. *Geochim. Cosmochim. Acta*, 1979, **43**, 1075–1090.
27. Thomson, J., Higgs, N. C., Wilson, R. R. S., Croudace, I. W., de Lange, G. J. and van Santvoort, P. J. M., Redistribution and geochemical behaviour of redox-sensitive element s around S1, the most recent eastern Mediterranean sapropel. *Geochim. Cosmochim. Acta*, 1995, **59**, 3487–3501.
28. Reitz, A., Thomson, J., De Lange, G. J. and Hensen, C., Source and development of large manganese enrichments above eastern Mediterranean sapropel S1. *Palaeoceanography*, 2006, **21**, PA3007; doi:10.1029/2005PA001169.
29. Plueger, W. L., Friedrich, G. and Stoffers, P., Environmental controls on the formation of deep-sea ferromanganese concretions. *Monograpohs Series on Mineral Deposits*, Gebruder Borntraeger, Berlin, 1985, vol. 25, pp. 31–52.
30. Sundby, B., Transient state diagenesis in continental margin muds. *Mar. Chem.*, 2006, **102**, 2–12; doi:10.1016/j.archem.2005.09.016.

ACKNOWLEDGEMENTS. Part of the work was carried out under the CSIR Network Program on RIDGE (COR0006). We thank the DOD, New Delhi (now MoES) for ship time. We also thank the officers and crew of *ORV Sagar Kanya* for their skillful operations and the shipboard scientific and technical party for support in sample and data collection during SK-114, SK-154 and SK-207 cruises. A.B.V. is grateful to Prof. R. Shankar, Mangalore University for carrying out MS measurements on sub-sections. We thank Prof. D. Chandrasekhram, IIT Bombay for helpful comments on the manuscript. Technical support given by G. A. Prabhu for XRD, S. Vijayan during geochronological analysis and P. Pawaskar in preparing the figures is acknowledged. This is NIO contribution no. 4516.

Received 1 September 2008; revised accepted 2 March 2009

A process for organic water

Vikram Soni[1], Ravi Mehrotra[1,*], P. S. Datta[2] and S. Chander[3]

[1]National Physical Laboratory (CSIR), K.S. Krishnan Road, New Delhi 110 012, India
[2]Nuclear Research Laboratory, Indian Agricultural Research Institute, New Delhi 110 012, India
[3]TERI School of Advanced Studies, Lodhi Road, New Delhi 110 003, India

We present a local, self-sustaining, natural and economic way to secure a quality drinking water resource for a town or city. Most local rainfed aquifers in the environs of cities suffer from long-term contamination by chemical waste – either fertilizers and pesticides or urban effluents. We propose a process by which such aquifers can be restored to quality. This is accomplished by first changing the land use of the catchment area of local aquifers to forest, and then by a yearly evacuation of water in the aquifer till quality is restored. A model is used to estimate that, typically, by yearly evacuation of the aquifer, pollution in the aquifer water is reduced to 10% of its initial value in 5–7 years. This is an organic process to purify the water in the aquifer. We also find that the area required for this falls within 10% of the total area of the city, well within the green area norm for a city.

Keywords: Chemical waste, green area, organic water, rainfed aquifers, yearly evacuation.

IT is common knowledge that our planet is faced with a major problem in the available water resources[1,2]. This problem has two dimensions:

(1) The first is with respect to the quantity of water available. With increasing population, the demand for water, both for human consumption and agriculture, has been steadily increasing. Also, the melting of glaciers, deforestation and general environmental degradation, in particular, of rivers, have cut the retentivity, flow and availability of water on the planet.

(2) The not so obvious problem, which is perhaps more serious, has to do with the quality of water, which has deteriorated over the last 50 years, so as to render most of it unfit for drinking. How has this happened?

Excessive urban migration has inflated cities beyond manageable limits, to produce such quantities of effluents so as to render both the local groundwater and rivers flowing by cities to be criminally polluted. This has happened mostly due to leaching of contaminants from landfills, indiscriminately disposed anthropogenic toxic waste, unplanned application of agrichemicals and surface runoff from farm lands[3].

More surprising is the state of groundwater in the rural areas which do not have waste-disposal problems like the metropolitan areas. The pollution here has occurred due to the heavy doses of fertilizers and pesticides used for modern agriculture. The cumulative effect has been to contaminate the near-surface groundwater base with fertilizers and pesticides. This pollution is long term and has no simple solution.

The USGS has extensive data available for the quality of groundwater for various kinds of land use across the country. One such set of data is shown in Figure 1 for the Long Island–New Jersey coastal drainages[4]. It is evident that the quality of water in the undeveloped areas is far superior to the one where there is urban or agricultural land use. The quality can only improve further for the case of a protected forest, where the root system of trees provides additional filtering of pollutants.

Quality drinking water is thus hard to come by except in wilderness areas, which are generally far away from the populations that require water. Transport of water from such areas to cities is then a high-entropy, high-cost, major pipeline project. Furthermore, transport of a fundamental and local resource like water is ecologically unsound and wasteful.

The other possibility for producing potable water is the technological fix of chemical treatment (reverse osmosis and resin), but this has the disadvantage of high cost, leaching of important healthy minerals – which yields only processed and not mineral water, and producing a sludge which causes a disposal problem. This makes it impractical for poor, underdeveloped and remote areas.

We now describe a process for purification of natural aquifers that occur in the environs of a human settlement, but have been cumulatively polluted by human activity over the years (we use the term 'human settlement' to mean any village/town/city and hereafter, we abbreviate it further to a 'settlement' throughout the text). The water stored in these aquifers is purified in the process and a local, self-sustained source of high-quality drinking water is created.

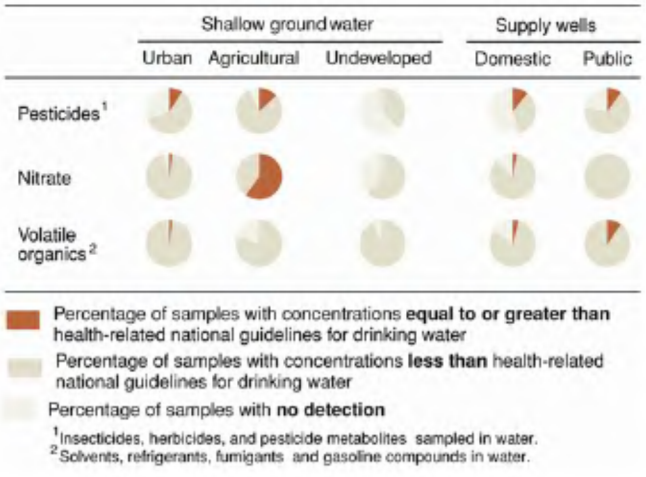

Figure 1. Selected indicators of groundwater quality for various kinds of land use in the Long Island–New Jersey coastal drainages.

*For correspondence. (e-mail: ravi@nplindia.org)

Using a conservative figure of 3 l per person per day, we get the annual requirement of drinking water for the settlement. Once aquifers with the appropriate recharge capacity have been located, we must create and protect forests on their entire catchment, so that the total recharge capacity is equal to or exceeds the requirement computed above. Further pollution can be eliminated by changing any urban or agricultural land use in the catchment to a protected forest area. This enables the water recharging the aquifer to be free from agricultural and other contaminants like fertilizers and pesticides (nitrates, phosphates, fluorides, etc.), and instead makes it rich in natural minerals.

A simple way to estimate the groundwater recharge for an area based on rainfall and pan evaporation data is presented elsewhere[5]. After estimating the total evaporation loss and subtracting it from the total rainfall, we find the balance available for recharge and run-off. For a large and heterogeneous area, the aquifer potential or recharge has to be determined from the hydrogeology of the area. This can be done using, for example, empirical data from the curve number technique, which gives the recharge from the porosity data of the local terrain.

Once the land use in the catchment area of the aquifer has been changed to forested land, our process of purification involves yearly evacuation of water in the aquifer by pumping out for agriculture (or other use) to a location outside the aquifer catchment. The efficacy of this method is illustrated using a simple but realistic model.

After annually pumping out the contaminated water in the aquifer for a period of 5–7 years, the fresh recharge flowing into the aquifer through the protected forest then gives us high-quality spring water ideal for drinking. We call this as 'organic water'. As outlined above, the process involves an integration of natural processes.

One of the most pressing issues in this process is the timescale in which the water in aquifer can be decontaminated and purified. We now turn to this. Once the land use is changed and no fertilizer is applied to the ground, the unpolluted rainwater will pick up contamination from the top sublayer, leaving it less polluted in its passage. The rainwater will then move to the next sublayer carrying some pollutant picked from the previous sublayer. Assuming the same initial pollutant concentration (uniform) in the sublayers, the concentration in this sublayer, after mixing with the incoming rainwater, will be more than that for one sublayer above. Thus, the pollution concentration gradient in the soil will be positive with depth. Every succeeding rain will keep lowering the concentration of the pollutant in the soil, thus washing it into the aquifer.

We shall consider this problem using a simple model shown schematically in Figure 2. This model needs some relevant parameters to be specified. We discuss below, stepwise, these parameters, details of the model and the results.

(i) We assume an unsaturated zone of porous soil of depth, H. This is simply the layer of soil that starts at the ground level and extends down till the subsoil level at which the aquifer begins. A unit volume in this layer fractionizes thus: m is the volume fraction of polluted water which we term specific moisture, s is the volume fraction of soil matter, leaving a fraction $(1 - m - s)$ as empty volume.

(ii) Rain falls on the ground, which is the top of this layer. On subtracting the loss due to evaporation and run-off the balance, which is the recharge rainfall, percolates down through it to the aquifer. We shall consider only soluble contaminants (as insoluble ones will not percolate down in the recharge). The model does not distinguish between contaminants.

(iii) We have a dilution model of pollution, in which we assume ideal mixing between the specific moisture in the soil and the inflowing rainwater. Thus, when a certain volume of rainwater enters a sublayer of the soil, the pollution concentration in the sublayer becomes the weighted average of the two.

(iv) The initial pollution concentration in the soil and its depth profile are inputs to the model. For simplicity and convenience in discussing the model, we take the initial concentration of pollutant to be uniform through the depth, H, of the unsaturated zone. However, the model equations apply to any given concentration profile.

(v) A difference equation for the above model can be written in the following way. Each rainfall event results in a recharge pulse of at most a few centimetres of water

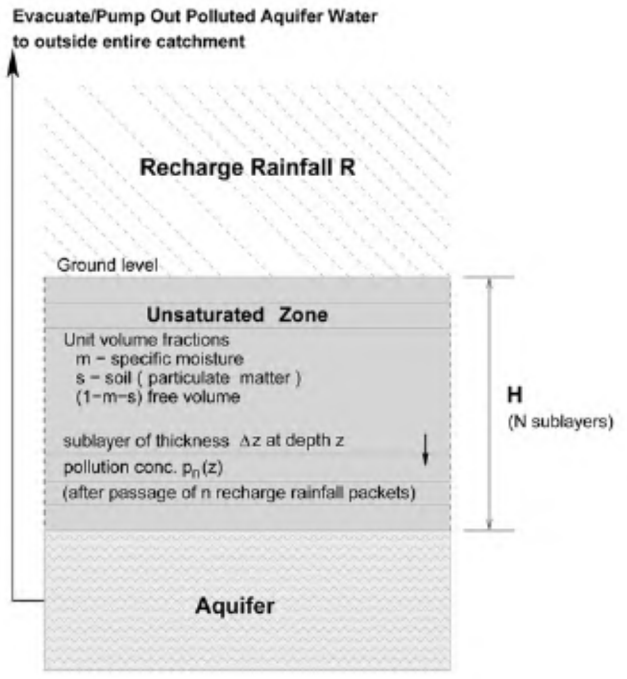

Figure 2. A schematic of the model for purification of unconfined aquifers.

percolating down into the ground. The total depth H is divided into N sublayers, each of depth $\Delta z = H/N$. Rainfall recharge is then divided into small packets of height $\alpha\Delta z$, such that the recharge water at most completely fills the empty volume in the thin sublayer. Thus, $\alpha_{\max} = 1 - m - s$. Choice of the size of recharge rainfall packet, and consequently the value of α is not important, as the results are independent of this.

Consider a thin horizontal sublayer of unit area and thickness Δz at depth z below ground. Let $p_n(z)$ be the pollution concentration in this thin sublayer at position z after n packets of recharge rainfall have passed through the sublayer. Recharge rainwater with volume $\alpha\Delta z$, carrying a pollution concentration $p_n(z - \Delta z)$, enters this sublayer from the sublayer above at $(z - \Delta z)$. The incoming recharge water mixes completely with the specific moisture in the sublayer, having pollution concentration $p_{n-1}(z)$, lowering the pollution concentration in the sublayer. With no sources or sinks of water in the sublayers, this mixing can be expressed mathematically as:

$$p_n(z) = \frac{mp_{n-1}(z) + \alpha p_n(z - \Delta z)}{m + \alpha}. \quad (1)$$

Given an initial pollution concentration profile, eq. (1) can be solved iteratively, as each packet of recharge rainfall percolates down the sublayers, to obtain the new profile of pollution concentration after the passage of the rainfall packet. The profile depends additively on the number of such packets. Thus, the heterogeneity of rainfall over the year does not play a role. Only the total recharge rainfall is of consequence. The new profile can be plotted, after a number of packets equivalent to the average total yearly rainfall have passed through the sublayers, to monitor the yearly pollution concentration profile. We, therefore, present the results in terms of the total effective annual recharge.

We have ignored effects of diffusion in deriving the above equations. Diffusion terms do not affect the average velocity of downward displacement of pollution. It is also straightforward to have the specific moisture m depend upon depth. In this case, m gets replaced by $m(z)$ in the above equation.

Our results are summarized by the simplistic piston model[6] and are consistent with it[7]. It states that purification is achieved when the total recharge inflow, which is the annual recharge multiplied by the number of years, is equal to the specific moisture, m, multiplied by the depth, H.

To understand this better we need to breakdown the hydrology of precipitation, P, into its various and distinct parts. Once rain falls on any area, first, there is surface evaporation loss, S. This depends on the climate and the soil. Next, we have to account for run-off and transpiration from the vegetal cover. For example, on flat agricultural land or flat pasture or woodland, the run-off is small, and for forests, transpiration is more than that for the pasture. On the other hand, on land that is contoured by slopes, a large portion of the balance goes in the run-off. Also, if the soil is impervious, like clay, run-off is dominant. Depending on their geographical location, aquifers present varying situations.

There are four main parameters in this estimate.

(1) Rainfall: (i) A rainfall, $P \sim 50$–60 cm, presents arid condition. This would apply, for example, to Delhi, where after surface evaporation, only 15 cm may be left for recharge, transpiration and run-off, of which we find 60% recharge for the forested catchment, or 9 cm of recharge. (ii) A rainfall, $P > 100$ cm (e.g. Bangalore, Pune, Dehradun) will have no more evaporation than in (i) above and could leave 75 cm for recharge, transpiration and run-off, of which as much as 30 cm or more may be available for recharge.

(2) The specific moisture or field capacity, m: (i) For sand, $m = 0.05$ (e.g. desert conditions in Rajasthan, Gujarat). (ii) For sandy loam as occurring around some areas in Delhi, $m = 0.15$. We shall use a typical average value of $m = 0.10$.

(3) The depth, H, of the unsaturated layer can vary from aquifer to aquifer. We have shallow aquifers in mind, which can vary from $H = 10$ to 30 m, and for our estimation we use an average value $H = 20$ m.

(4) The specific characteristics of an aquifer: The ratio of the catchment area to the aquifer area, r. Assuming R to be the normal recharge (in cm), we can define a catchment augmented effective recharge $E_r = R \times r$.

Based on the above model, we present below results for a typical situation with the following parameters: Specific moisture $m = 0.1$, soil fraction, $s = 0.2$, effective recharge (annual), $E_r = R \times r = 35$ cm, depth of aquifer $H = 20$ m.

The initial groundwater pollution is assumed to be uniform. A yearly plot of the groundwater pollution profile is shown in Figure 3. The curves correspond to profiles

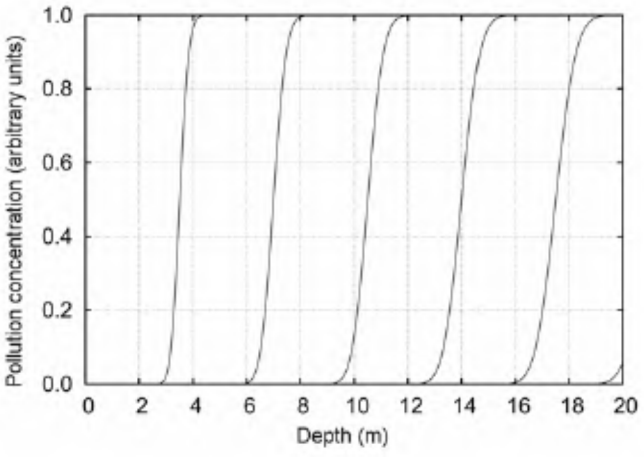

Figure 3. Groundwater pollution profile as a function of depth below ground into the unsaturated zone at yearly intervals after flushing with recharge rainwater. The aquifer is 20 m deep, specific moisture $m = 0.1$, soil fraction $s = 0.2$ and effective recharge $E_r = 35$ cm. The curves from left to right correspond to profiles after one to six years respectively.

after each consecutive year respectively. For the given aquifer characteristics, in 6 years the aquifer water pollution drops to about 10% of the original. In the absence of diffusion terms, the change in the slope of the profiles is an artifact due to a finite chosen value of the number of sublayers N and dz.

Implementation of such a scheme requires the following:

(1) An intervention in public policy that for towns and cities, all nearby aquifer catchments be declared vital state assets and be protected. To maintain water quality, the entire catchment area of the aquifer has to be protected – this area must fall outside the urbanized zone.

(2) Cooperatives or water companies to step in and manage drinking water services derived from these aquifers. This is highly profitable economically. The land we are talking about is strictly agricultural with its land use fixed and thus cannot be valued as regular real estate. The main cost is the renumeration to farmers who own the land. A renumeration of even four times the maximum agricultural income from the land, makes hardly a dent in the earnings from the service.

(3) A period of 5–7 years for such quality drinking water sources to be operational.

The main advantages of the process are that there is no use of chemical technology and no toxic waste is produced. It uses a natural percolation process for rainwater to come into the aquifer. Foresting the catchment provides good foliage and humus to supplement water retentivity. The roots of the trees consolidate the soil and provide additional natural filtration to enhance the quality of the water. Run-off and erosion are reduced, thereby increasing the groundwater recharge. Hence recharge estimates in the examples are lower bounds. Natural, green wooded area, which is less than 10% of the city area, is required for this purpose. This falls neatly into the urban planning norm of having about 20% green area in a city. Due to it being a natural process, the main costs involve the remuneration given to farmers whose land has been converted to wooded area. Even if the estimated remuneration is about five times the annual income of the farmer from the said land, the cost of generating pure drinking water of high quality is extremely cost effective compared to the ecological and financial costs involved in bottling and transporting water from remote, unpolluted wilderness sources, such as mountain streams, or purification of water by chemical or osmotic process.

At present, it is estimated that almost half the world's population has no access to good drinking water. This is considered an essential cause of several debilitating water borne diseases. This is the primary component in preventable human mortality. At a cost of US$ 0.02/l, the annual cost of providing 2 litres of good drinking water per day per person works out to approximately US$ 15 billion for every billion people. The UNEP experts have estimated[8] the cost of providing safe drinking water and proper sanitation to everyone in the world by 2025 at US$ 180 billion. Needless to say, the present cost in terms of health is much more. Providing a simple, natural, low cost, local and self-sustaining solution to the drinking water problem is vital. Organic water will do just that.

1. Gleick, P., *The World's Water 2008–2009: The Biennial Report on Freshwater Resources*, Island Press, Washington DC, 2008.
2. Witkowski, A. J., Kowalczyk, A. and Vr, J. (eds), *Groundwater Vulnerability, Assessment and Mapping: Selected Papers from the Groundwater Vulnerability Assessment and Mapping International Conference: Ustrón, Poland, 2004*, Routledge, New York, 2007.
3. Datta, P. S., *Groundwater Situation in Delhi: Red Alert*, Nuclear Research Laboratory Publication, IARI, New Delhi, 1999.
4. http://water.usgs.gov/pubs/circ/circ1201
5. Soni, V., The carrying capacity of a city based on water. *Econ. Political Wkly*, 8 November 2003, pp. 4745–4749.
6. Green, W. H. and Ampt, G. A., Studies on soil physics, part I, the flow of air and water through soils. *J. Agric. Sci.*, 1911, **4**, 1–24.
7. Dahiya, I. S., Singh, M., Richter, J. and Singh, M., Leaching of soluble salt during infiltration and redistribution. *Irrig.* Sci., 1984, **5**, 15–24.
8. http://news.bbc.co.uk/1/hi/sci/tech/2293621.stm

ACKNOWLEDGEMENTS. We thank Gautam Soni and Kusum Chauhan for their interest and remarks on the subject. We also thank Anasuya Weil, Parveen Anand and Sunita Sreedaran for help.

Received 31 January 2008; revised accepted 6 March 2009

Role of sorption properties and water status in control of seed longevity patterns

D. Vijay[1,3,*], M. Dadlani[1] and Shantha Nagarajan[2]

[1]Division of Seed Science and Technology, and
[2]Nuclear Research Laboratory, Indian Agricultural Research Institute, New Delhi 110 012, India
[3]Present address: A.P. Rice Research Institute and RARS, Maruteru 534 122, India

The longevity behaviour of two oil-rich seeds, soybean (*Glycine max* (L.) Merrill) and safflower (*Carthamus tinctorius*) were compared using their water absorption properties. The nuclear magnetic resonance characterization of water in different moisture equilibrated seeds was studied in relation to the viability of both the crops. The component analysis of the transverse relaxation showed the presence of different components in soybean and safflower at corresponding relative humidity. Even though a more deleterious third component (structurally bound water) was observed at higher relative humidity in both the crops, the dif-

*For correspondence. (e-mail: vijaydunna@gmail.com)

ference in its relative population clearly shows the linkage between molecular mobility of water and longevity. The dehydration and rehydration isotherms studied under the ambient relative humidity pointed towards the possible development of extra polar sites in soybean along with the varied behaviour of these two seeds under fluctuating relative humidity conditions, which is a common phenomenon in ambient storage conditions. Thus, the present study emphasizes that the sorption properties along with the structural partitioning of the seed water, which are influenced by the chemical composition of seed, play an important role in the longevity behaviour of seeds besides other factors like lipid peroxidation.

Keywords: Dehydration–rehydration isotherms, nuclear magnetic resonance, safflower, seed deterioration, soybean.

THE deterioration of seeds, resulting in the loss of vigour and viability is inexorable[1]. Storage temperature and seed moisture content are the most important factors controlling seed longevity. The physical state of water in the seeds during storage or prior to pre-germination imbibition strongly influences the staying quality and success of subsequent germination. The importance of different properties of water in determining seed longevity has also been recognized[2]. Deteriorative reactions proceed more rapidly if the moisture content is high in the seed, and consequently the moisture status would constitute a threat to longevity. Water also acts as a solvent for most of the biochemical reactions, and hence loss of this solvent will reduce the diffusion rate of solute substances to an active site and thereby reduce the pace of deleterious metabolic activities. With decreasing water content the molecular mobility reaches a minimum, thereby increasing the seed longevity[3].

Nuclear magnetic resonance (NMR) spectroscopy is a non-destructive method used to study the water status in different biological systems. Seed water status refers to the measurement of water properties in relation to the seed, and is used in a relative sense[4]. Water status can be described either by measuring the moisture levels of tissue water content or by measuring the energy status of cell water. Moisture levels of seeds are an important determinant of seed longevity[5]. The longitudinal and transverse components of NMR relaxation times of protons can be used in understanding both the compartmentation and transport of water in tissues of plants as well as seeds[6]. The differential mobility of water molecules can be determined using the difference in their relaxation rates, which also enables us to calculate their relative amounts in the tissue[7–9]. The NMR relaxation times have been used for the characterization of seed water in different species[9–11]. The water in dry seeds, mostly in the bound state, is structured and non-freezable[12], but the storage quality of seeds is largely dependent on free or bulk water which fluctuates with the relative humidity of the surrounding air[8].

The difference in the moisture sorption patterns and the thermodynamic status of water in seeds which controls the seed deterioration reactions[1,4], may differ considerably between seeds of different species. The chemical compositions of seeds appear to play an important role in determining the general storability behaviour of seeds of different species, though information on comparative performance of seeds having different chemical composition is scanty. With lipid peroxidation playing a critical role in seed deterioration, seeds containing high levels of polyunsaturated fatty acids are expected to exhibit poorer longevity[13,14]. In the present study two oil-rich seeds, soybean and safflower, having different storability were compared with an objective of an in-depth understanding of the influence of water sorption properties on the deterioration patterns.

For the present study, seeds of soybean (*Glycine max* (L.) Merrill) cv JS 335 and safflower (*Carthamus tinctorus*) cv A-1 were obtained within three months of harvest from the National Research Centre for Soybean, Indore, and University of Agricultural Sciences, Dharwad respectively. The physically pure seeds were taken and the protein, carbohydrate and oil contents were estimated according to standard procedures[15], for an overview of the chemical composition of these two crop seeds. The seeds were packed in polythene bags (700 gauge) under ambient conditions of storage, with an average temperature of 25 ± 2°C (max 40°C and min 13°C) and average relative humidity (RH) of 65 ± 2% (max 93% and min 14%) up to one year.

The germination percentage was measured for both the crop seeds using the between-paper method, in four replications of 50 seeds each at 25°C following the standard ISTA method[16]. The germination test was conducted initially and at three months interval up to one year under ambient storage conditions.

Three sets of soybean and safflower seeds having an initial moisture content of 10.5 and 6.8% respectively, were weighed accurately to 30 g each. Seeds were taken in perforated muslin bags and equilibrated over saturated salt solutions at 25°C in air-tight desiccators. RH of 30, 50, 70 and 90 was obtained with the saturated salt solutions[17,18]. Seeds incubated for equilibration were weighed daily until constant weight was attained on four successive weightings (at which point the seeds seemed to be equilibrated), and absorption curves were drawn with equilibrium moisture content on the *Y*-axis and RH on the *X*-axis. The seed moisture content and spin–spin relaxation time (T_2) were measured as follows.

Seed moisture content was determined in three replicates by oven-drying the seeds at 103°C for 17 h to constant weight[16]. The moisture content (%) was calculated as $((W_1 - W_2)/W_1) \times 100$, where W_1 is the initial weight of the seed (g) and W_2 the final weight of the seed after drying (g).

NMR relaxation times were measured in six replications on moisture-equilibrated seeds. The seeds were

placed in 10 mm diameter glass tubes with a column height of about 2 cm and corked immediately to avoid exchange of moisture with the surrounding atmosphere. The tubes were then placed in the probe of Bruker NMS 120 pulsed NMR spectrophotometer according to the procedure described by Krishnan[8].

Seed water spin–spin relaxation time (T_2) was measured using Brucker NMS 120 minispec NMR analyser at 20 MHz and ambient temperature of 25°C, by studying the decay of the transverse component of magnetization using the Carr-Purcell Meiboom Gill method[19]. Seed materials were tested with the following settings. Number of datapoints, 150; pulse separation, 0.5 ms; dummy echo, 3, and number of scans, 4. The T_2 values were determined by measuring the exponential decay of the signal and the in-built program of the instrument was used to calculate this. According to Ratkovic[10], three different water components can be identified in seed systems using spin–spin relaxation time. The three components of T_2 (T_{2a}, T_{2b} and T_{2c}) are given by the equation

$$M_t = C_a[\exp(-t/T_{2a})] + C_b[\exp(-t/T_{2b})] + C_c[\exp(-t/T_{2c})],$$

where C_a, C_b and C_c are related to the relative populations of the three components[20,21]. The components of spin–spin relaxation were analysed using least square fit analysis in the region of specified limits using a computer program[22].

The procedure followed to estimate the hysteresis loop through moisture absorption and desorption isotherms was modified after Moharir and Nam Prakash[23]. Two replications of 100 seeds each of soybean and safflower were weighed separately and hydrated in a closed desiccator at 100% RH and 27°C for conditioning or hydration of seeds. The increase in weight was recorded after 2, 4, 6, 24, 26, 28, 30 and 48 h. The hydrated seeds were then kept in an open petri plate of 6″ diameter and left to be dried at 27°C and ambient RH (60 ± 2%). The decrease in weight was recorded after 2, 4, 6, 24, 26, 28, 30 and 48 h. This is termed as the dehydration cycle. The dehydrated seeds were again transferred to 100% RH at 27°C and their weight was recorded at intervals as before. This is the rehydration cycle. By plotting the dehydration and rehydration values at each interval, the dehydration–rehydration curve was drawn.

The major chemical constituents of the seed, i.e. carbohydrates, proteins and lipids were determined in two replications of 10 g seed of soybean and safflower at a moisture content of 9.39 and 7.49% respectively. The safflower seed had high carbohydrate content of 48% followed by 38% oil content and 10% protein content, whereas the soybean seed had 37% carbohydrates, 19% oil and 39% protein. Thus, even though both are rich in oil their chemical composition was different, with soybean being a protein oil-rich and safflower a starch oil-rich seed. The germination was recorded at three months interval up to one year under ambient laboratory conditions with an average temperature of 25 ± 2°C (max 40°C and min 13°C), and average RH of 65 ± 2% (max 93% and min 14%). A gradual decline was observed during this period, with germination falling from 92–95 to 66–79% in soybean and safflower respectively. Decline in germination was rapid in soybean beyond 6 months of storage which coincided with higher RH and temperature conditions, whereas it was steady and gradual in safflower throughout (Figure 1).

The equilibrium moisture content was determined at 30, 50, 70 and 90% RH at 25°C in soybean and safflower seeds having initial moisture content of 6.8 and 5.4% respectively. The equilibrium moisture content (EMC) values attained by both the seeds were almost equal up to 50% RH; at higher RH levels the soybean seeds attained higher EMC, which was almost 1.5 times higher than that of safflower. The absorption curves were of sigmoidal type for both the species, albeit a steeper slope was observed for soybean (Figure 2). Total increase in moisture content with respect to initial moisture content was 3.5 times in soybean and 2.3 times in safflower.

The spin–spin relaxation time T_2 (ms) of seeds equilibrated at different RH levels showed a progressive decrease with increase in EMC values (Table 1). The T_2 values varied from 84 to 65 ms in soybean, as against 114 to 103 ms in safflower. At a given RH or at similar EMCs (up to 50% RH), the spin–spin relaxation times were higher for safflower seeds than for soybean seeds.

T_2 was further partitioned to determine different components of seed water and their relative populations at increasing levels of RH. Initially only two components were observed up to 70% RH. At 90% RH, three components were found in both species. The component with long relaxation time (T_{2a}) increased with increase in RH

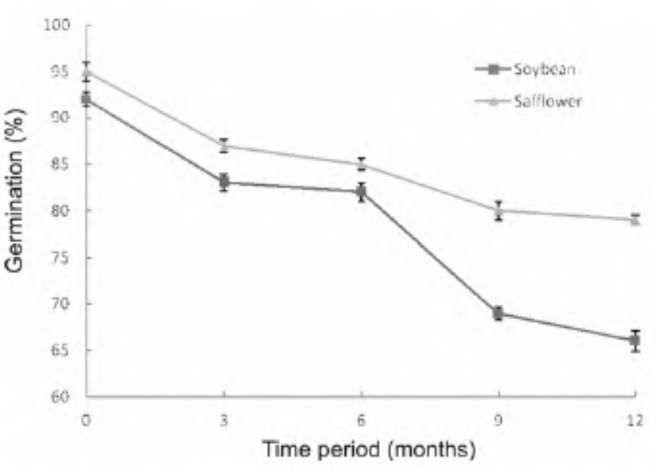

Figure 1. Germination (%) at 25°C of soybean and safflower seeds stored under ambient storage conditions of average temperature 25 ± 2°C (max 40°C and min 13°C) and an average relative humidity of 65 ± 2% for one year period.

up to 70% (Table 2). The relative populations of two components (T_{2a} and T_{2b}) were not altered with increase in RH (70%) but at 90% RH there was an alteration in the populations in both soybean and safflower seeds. Interestingly, the proportion of the slow relaxing component was higher in safflower at any given RH level (Figure 3).

The moisture adsorption and desorption patterns of soybean and safflower were determined on the basis of dehydration and rehydration behaviours under vapour-saturated atmospheres. The moisture content of soybean and safflower seeds reached 14.3 and 18.8% after conditioning for 48 h at 100% RH and 27°C. These were then subjected to air-drying for different periods. At the end of the dehydration cycle of 48 h at ambient RH and temperature, the moisture content of these two kinds of seeds was found to be 10.6 and 5.8% respectively. A second cycle of rehydration at 100% moisture vapour-saturated condition resulted in an increase in seed moisture content to 17.5 and 18.4% in soybean and safflower seeds respectively. Thus, after the rehydration cycle the safflower seeds attained almost the same moisture content as that recorded in first hydration cycle, whereas soybean seeds gained more moisture upon rehydration. The difference in moisture content attained at saturation after the first (hydration) and second (rehydration) cycles of moisture vapour conditioning was 3.2% in soybean and 0.4% in safflower. Thus, even though the difference in moisture absorption upon rehydration following dehydration was more in soybean, interestingly, there was a larger area under the hysteresis loop in the case of safflower (Figure 4).

The pattern of loss of germination under ambient conditions of storage was similar in the two species up to 6 months of storage, which coincides with the low moisture content of soybean and safflower seeds (7.83 and 6.94% respectively) during this period. After 9 months of storage a marked difference was noted in the moisture content and germination of soybean and safflower seeds, which was even more pronounced after 12 months of storage, by which time the moisture content and germination of soybean were 11.13 and 66% respectively, compared to 8.96 and 79% in safflower. Survival of seeds under ambient storage depends more on their moisture content than on any other factor[24]. This has been attributed to the notion that physiological reactions, deleterious to seed longevity, increase with the increase in seed moisture content, in addition to influencing the incidence and survival of storage pathogens. In the present study, a clear-cut difference was observed in soybean and safflower seeds with respect to germination (Figure 1), patterns of moisture sorption, moisture equilibrium (Figure 2) and physical status of seed water, determined by partitioning of different components of seed water at different levels of relative humidity, and retention and release of moisture by the seed in a fluctuating environment (Figure 4).

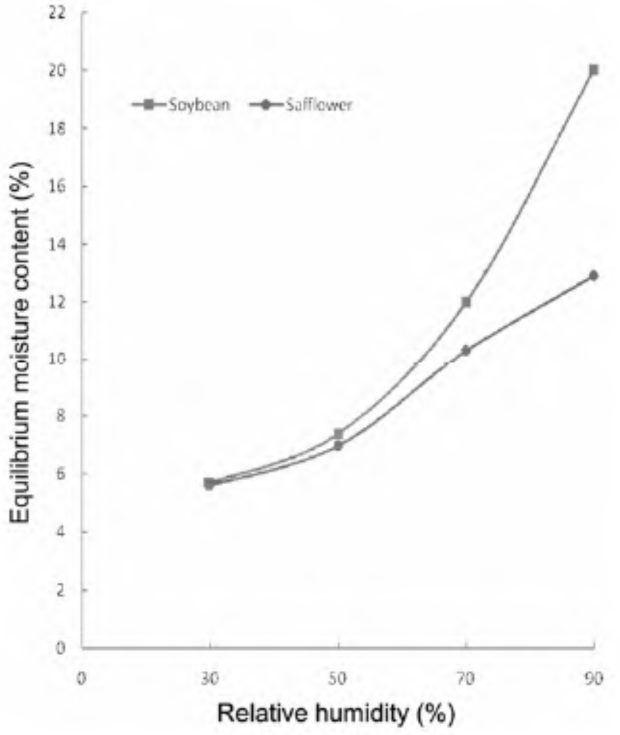

Figure 2. Absorption equilibrium moisture content curves of soybean and safflower seeds at different RH levels at 25°C.

Table 1. Equilibrium moisture content (EMC) and spin–spin relaxation times (T_2) of soybean and safflower seeds at different relative humidity (RH) levels

	Soybean		Safflower	
RH (%)	T_2 (ms)	EMC (%)	T_2 (ms)	EMC (%)
30	84 ± 0.9	5.7	114 ± 2	5.60
50	82 ± 1	7.4	111 ± 2	6.96
70	80 ± 1	11.98	106 ± 2	10.28
90	65 ± 2	20	103 ± 2	12.92

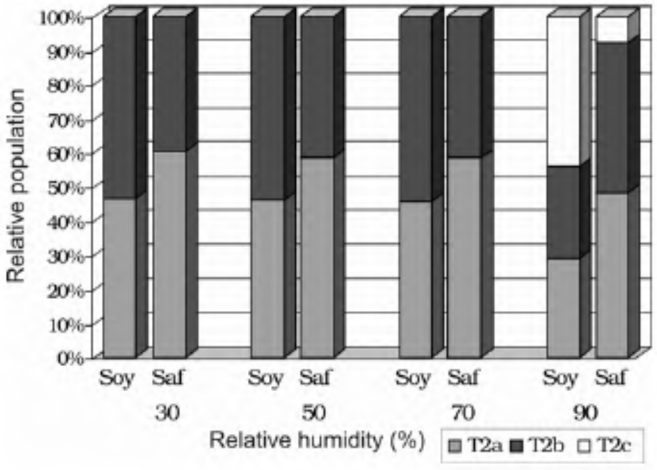

Figure 3. Relative population of T_2 components (T_{2a} represents extracellular free water, T_{2b} cytoplasmic bulk water and T_{2c} structurally bound water) at different RH levels in soybean (Soy) and safflower (Saf) seeds.

Table 2. Different components of spin–spin relaxation time (T_2) of soybean and safflower seeds at different RH levels

	T_{2a} (ms)		T_{2b} (ms)		T_{2c} (ms)	
RH (%)	Soybean	Safflower	Soybean	Safflower	Soybean	Safflower
30	575.2	530.4	46.2	50.7	–	–
50	598.2	530.6	47.7	50.8	–	–
70	709.4	555.3	50.6	51.0	–	–
90	650.4	726.8	47.3	57.2	3.15	1.7

T_{2a}, T_{2b}, T_{2c} are three different components of T_2 (T_{2a} represents extracellular free water, T_{2b} cytoplasmic bulk water and T_{2c} structurally bound water).

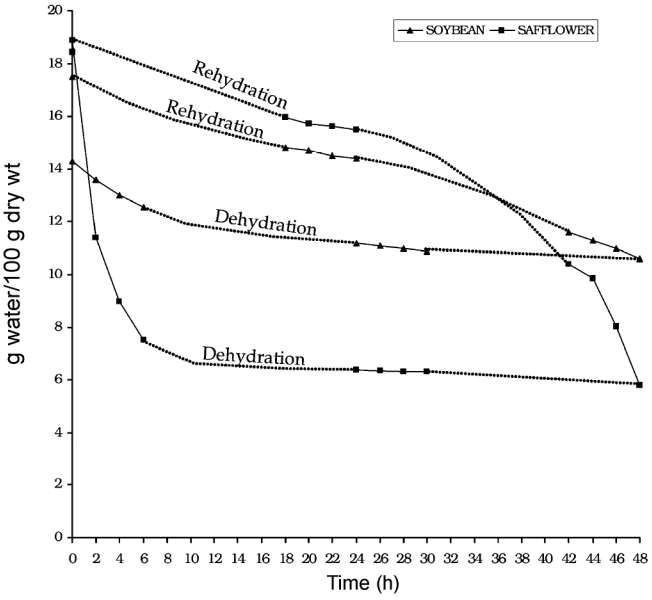

Figure 4. Hysteresis loop of dehydration and rehydration cycles measured as gram water/100 g dry wt of seeds over a time period in soybean and safflower seeds.

The pattern of moisture absorption by the soybean and safflower seeds was similar in the two crops up to 50% RH, but it shot up dramatically in soybean at RH of 70% and above, whereas the rise remained slow and gradual in safflower, resulting in a difference of about 7% in the EMC at 90% RH between the two crops (Figure 2). The higher absorption values in soybean can be attributed to higher amount of macromolecules other than lipids, viz. proteins and starch, which are hygroscopic in nature[24]. Walters[1] compared the results from studies made by different workers on water-sorption isotherms of seeds of a number of crop species having different chemical compositions, viz. pea, soybean, lettuce, peanut and sunflower, and noted that at similar levels of RH protein oil-rich seeds of soybean achieved a significantly higher EMC compared to that of lettuce, peanut and sunflower respectively, whereas high protein, low oil pea seed attained EMC even higher than that of soybean. Walters inferred that the relative hygroscopicity of the major seed constituents, i.e. proteins, starch and lipids, plays a major role in their sorption behaviour. The present study has clearly established this point under identical conditions of RH and temperature by examining the pattern of water sorption in two different crop species, i.e. soybean and safflower. Results of the present study also indicate that more than the absolute moisture content attained by the seed, it is the proportion of various seed water components that plays a greater role in seed deterioration. T_2, which represents the mobility of water molecules within the seed, is modified by seed structure and chemical constituents of its tissues. The T_2 values are influenced by many factors such as proton relaxation, cell size and structure, chemical composition and viscosity of cellular constituents, and their magnetic susceptibility[9]. The delicate balance between the total water content, macroscopic and microscopic distribution of water in different sites, macromolecule–water interactions and exchange between different water phases (liquid, glass or gaseous) determines the NMR relaxation times of seed tissue water. Soybean seed with its high protein + carbohydrate content showed a rapid moisture uptake at higher RH, and a slow release upon dehydration, which probably was due to the development of additional polar sites of attachment of water molecules in it. At high moisture content, changes will occur in the properties of macromolecular structure and hence, in the status of water in their vicinity[25]. These irreversible macromolecular structural changes can advance the process of deterioration, resulting in the non-viability of the seed. In the present study, T_2 decreased with increase in moisture content at different RH levels. The reduction in T_2 could be due to the increase in interaction between water and the macromolecules in the tissues[26]. Further, T_2 was partitioned into two fractions based on the relaxation time up to 70% RH. The slow relaxing fraction with long relaxation time was identified as extracellular free water, since the macromolecular concentration was comparatively less in the extracellular space of the tissues[8,10]. The fast relaxing T_2 fraction was generally identified as intracellular bulk water due to its short relaxation time[20]. At 90% RH, with the increase in EMC level, interestingly, a third component, T_{2c}, appeared in both soybean and safflower seeds. Based on its shortest relaxation time, it was identified as macro-

molecular-bound water. This kind of tissue water partitioning was earlier followed by many workers[9,20,21]. In the present study, it was significant to note that a larger proportion of seed water content in soybean remained as cytoplasmic bulk water, whereas in safflower the major proportion of total seed water content remained as extracellular free water, which could be rapidly released upon dehydration. At RH above 70%, the EMC attained by soybean seed was nearly 65% higher than that of safflower, of which nearly more than 30% was found to be in the bound form as against less than 10% in safflower (Figure 3). This is of a significant relevance during deterioration, as the nature and kinetics of chemical reactions are greatly influenced by the state of water, rather than the absolute water content within the seed[1].

The phenomenon of hysteresis, which occurs in absorptive substances with a high degree of structural rigidity, was examined on the desorption and reabsorption patterns of the two species. Due to its rapid dehydration in the initial stages and virtual lack of any moisture gain (over the initial level) during rehydration, safflower seeds showed a larger hysteresis loop than soybean (Figure 4). The faster dehydration seen in safflower could possibly be the result of a larger proportion of the seed water content remaining as extracellular free water than the cytoplasmic bulk water as found by NMR T_2 partitioning and needs further confirmation. The gain of excess moisture by soybean seeds, upon rehydration may be due to appearance of additional polar sites for bound water at higher RH as a result of tissue swelling[27]. The ability to readily release moisture at a lower external RH and gain slowly at a higher one, as in the case of safflower, is a property favourable for better seed longevity. Discrete changes in the proportion of seed water also suggested that seed ageing reactions were regulated by the thermodynamic status of water in the seeds[12,28].

Thus differential absorption and desorption patterns of soybean and safflower seeds, coupled with differential partitioning of water components in the two species due to their characteristic chemical constituents, are identified as one of the key factors contributing towards better longevity of safflower compared to soybean seeds under fluctuating environmental conditions (temperature and RH), particularly at RH above 70%.

1. Walters, C., Understanding the mechanisms and kinetics of seed ageing. *Seed Sci. Res.*, 1998, **8**, 223–244.
2. Williams, R. J., Methods for determination of glass transitions in seeds. *Ann. Bot.*, 1994, **74**, 3–12.
3. Vertucci, C. W. and Roos, E. E., Theoretical basis of protocols for seed storage. *Plant Physiol.*, 1990, **94**, 1019–1023.
4. Vertucci, C. W., Roos, E. E. and Crane, J., Theoretical basis of protocols for seed storage III. Optimum moisture contents for pea seeds stored at different temperatures. *Ann. Bot.*, 1994, **74**, 531–540.
5. Cromarty, A. S., Ellis, R. H. and Roberts, E. H. (eds), In *The Design of Seed Storage Facilities for Genetic Conservation*, International Bureau of Plant Genetic Resources, Rome, 1980.
6. Ratcliffe, R. G., *In vivo* NMR studies of higher plants and algae. *Adv. Bot. Res.*, 1994, **20**, 44–123.
7. Van As, H., NMR in horticulture: *In situ* plant water balance studies with NMR. *Acta Hortic.*, 1992, **304**, 103–112.
8. Krishnan, P., Nagarajan, S., Dadlani, M. and Moharir, A. V., Characterisation of wheat (*Triticum aestivum*) and soybean (*Glycine max*) seeds under accelerated ageing conditions by proton nuclear magnetic spectroscopy. *Seed Sci. Technol.*, 2003, **31**, 541–550.
9. Krishnan, P., Joshi, D. K., Nagarajan, S. and Moharir, A. V., Characterization of germinating and non-viable soybean seeds by nuclear magnetic resonance (NMR) spectroscopy. *Seed Sci. Res.*, 2004, **14**, 355–362.
10. Ratkovic, S., Proton NMR of maize seed water: the relationship between spin-lattice relaxation time and water content. *Seed Sci. Technol.*, 1987, **15**, 147–154.
11. Ridenour, C. F., Xiong, J. and Maciel, G. E., Investigation of germination and ageing in Moravian III barley grain by nuclear magnetic resonance. *Biophys. J.*, 1996, **70**, 511–531.
12. Leopold, A. C. and Vertucci, C. W., Moisture as a regulator of physiological reactions in seeds. In *Seed Moisture* (eds Stanwood, P. C. and McDonald, M. B.), Crop Science Society of America, Wisconsin, 1989.
13. Agrawal, P. K., Relative storability of seeds of ten species under ambient conditions. *Seed Res.*, 1980, **8**, 94–99.
14. Dadlani, M., Release of volatile compounds by soybean (*Glycine max*. L. Merrill) seeds and its effect on vigour and viability. *J. Plant Biol.*, 1999, **26**, 155–159.
15. Agrawal, P. K. and Dadlani, M. (eds), In *Techniques in Seed Science and Technology*, South Asian Publishers, New Delhi, 1987, pp. 187.
16. International Seed Testing Association (1999). International rules for seed testing. *Seed Sci. Technol.* (*Suppl.*), 1999, **27**, 333.
17. Rockland, L. B., Saturated salt solutions for static control of relative humidity between 50°C and 400°C. *Anal. Chem.*, 1960, **32**, 1375–1376.
18. Vertucci, C. W. and Roos, E. E., Theoretical basis of protocols for seed storage II. Influence of temperature on optimum moisture levels. *Seed Sci. Res.*, 1993, **3**, 201–213.
19. Snaar, J. E. M. and Van As, H., Probing water compartments and membrane permeability in plant cells by ^{1}H NMR relaxation measurements. *Biophys. J.*, 1992, **63**, 1654–1658.
20. Di Nola, A., D'Ubaldo, A., Fracassi, M. and Brosio, E., NMR study of seed hydration with deuterated water. Dependence of proton signals on hydration level. *Cell. Mol. Biol.*, 1991, **37**, 9–13.
21. Brosio, E., Di Nola, A. and Verzegnassi, B., NMR study of seed hydration: Effect of pH and ionic strength on water uptake of soaked cowpeas. *Cell. Mol. Biol.*, 1993, **39**, 193–198.
22. Nagarajan, S., Pandita, V. K., Joshi, D. K., Sinha, J. P. and Modi, B. S., Characterization of water status in primed seeds of tomato (*Lycopersicon esculentum* Mill.) by sorption properties and NMR relaxation times. *Seed Sci. Res.*, 2005, **15**, 99–111.
23. Moharir, A. V. and Nam Prakash, Moisture desorption and absorption isotherms for seeds of some cultivars of *Triticum aestivum* and *Triticum durum* wheat. *Curr. Sci.*, 1995, **68**, 316–326.
24. Justice, O. L. and Bass, L. N., *Principles and Practices of Seed Storage. USDA Agriculture Handbook* (eds Justice, O. L. and Bass, L. N.), Government Print Office, Washington, DC, 1978, p. 506.
25. Millard, M. M., Veisz, O. B., Krizek, D. and Line, M., Thermodynamic analysis of physical state of water during freezing in plant tissue based on the temperature dependence of proton spin-relaxation. *Plant Cell Environ.*, 1996, **19**, 33–42.
26. Kaku, S., Monitoring stress sensitivity by water proton NMR relaxation times in leaves of Azaleas that originated in different ecological habitats. *Plant Cell Physiol.*, 1993, **34**, 535–541.

27. Abdul-Baki, A. A. and Anderson, J. D., Viability and leaching of sugars for germinating barley. *Crop Sci.*, 1970, **10**, 31–34.
28. Roberts, E. H. and Ellis, R. H., Water and seed survival. *Ann. Bot.*, 1989, **63**, 39–52.

ACKNOWLEDGEMENTS. D.V. is grateful to CSIR, New Delhi for awarding Senior Research Fellowship during the period of this work. We thank Dr D. K. Joshi, Nuclear Research Laboratory, IARI, New Delhi, for technical help during NMR analysis. The study was supported by the National Agricultural Technology Project (ICAR) under the Team of Excellence in Seed Technology.

Received 16 April 2008; revised accepted 19 February 2009

Species and site effects on leaf traits of woody vegetation in a dry tropical environment

S. K. Pandey, Hema Singh* and J. S. Singh

Department of Botany, Banaras Hindu University, Varanasi 221 005, India

Selected leaf traits (leaf area, leaf weight, specific leaf area and chlorophyll content) from eight woody species at four sites in the dry tropical Vindhyan forest were investigated in order to assess their variability across species and site conditions. The morphological traits such as leaf area and leaf weight were more variable than biochemical traits such as chlorophyll content. There was significant effect of species and site, and the site × species interaction was also significant for all traits. These traits were correlated except for specific leaf area, which was independent of leaf area. A combination of traits could discriminate between the sites. Between-site variability in leaf traits was smaller (1.3–1.5-fold) than between-species variability (1.7–12.5 fold). The larger inter-species variability reflects marked genotypic variability in the leaf traits, while the smaller between-site variability reflects phenotypic plasticity leading to adaptation to site conditions.

Keywords: Dry tropical forest, inter-species variability, leaf traits, woody species.

LEAF traits are often cited as the principal traits to relate plant resource use, biomass and ecosystem functioning[1–4]. In addition, these traits are easy to quantify and convenient to compare among a large number of plant species. Leaf traits may be divided into two groups: functional traits and structural traits. Functional traits reflect the index of plant growth and metabolism. On the other hand, structural traits are indexes of biological characteristics of different plant species, and reflect the adaptation strategies of plants to the environment. These traits, among others, include leaf area, leaf dry weight, specific leaf area (SLA) and chlorophyll content. SLA is the ratio of leaf area to leaf dry weight and, being strongly correlated with relative growth rate, maximum rate of photosynthesis[3] and competitive ability, is often considered a key trait linked to plant functioning[5–8]. It has been argued that SLA can provide important clues regarding future changes in community composition due to global change, if dryness is going to be altered in much of the tropics. The high-SLA leaves are productive[6,9] but are necessarily also short-lived and vulnerable to herbivory[10,11]. On the other hand, low-SLA leaves perform better in resource-poor environments[7].

Leaf area plays an important role in light interception, water and nutrient use, growth and yield potential[12–14]. Leaf size and SLA decline along gradients of decreasing moisture and/or nutrient availability[15–20]. Lower SLA, due to thicker and/or denser leaves contributes to long leaf survival, nutrient retention, and protection from desiccation[21], whereas small leaf size reduces boundary layer resistance, and helps maintain favourable leaf temperatures and higher photosynthetic water-use efficiency under the combination of high solar radiation and low water availability[22,23].

Chlorophyll is the most important pigment for photosynthesis[24–26]. Chlorophyll concentration in leaves and canopies can be an indicator of photosynthetic capacity, developmental stage, plant productivity, environmental stress and nutrient management[27–30]. Measurement of leaf chlorophyll content is also an indirect approach to estimate soil nitrogen[31–33].

Since the leaf traits are considered important for understanding vegetation response to a broad range of environmental factors, we examined four leaf traits, viz. leaf area, leaf weight, SLA and chlorophyll content in eight woody species on four sites of a dry tropical forest in the Vindhyan highland. We addressed the questions: (i) How much do the woody species occurring in a dry tropical environment differ in these leaf traits and how much are these leaf traits affected by site conditions? (ii) Can a combination of these leaf traits across species discriminate between the sites?

The study was conducted on four sites, viz. Ranitalli, Neruiadamar, Bokrakhari and Hathinala of the Vindhayan dry tropical region (21°29′–25°11′N lat.; 78°15′–84°15′E long.), Sonbhadra District, Uttar Pradesh in 2008. The elevation above the mean sea level ranges between 313 and 483 m. The area experiences a tropical monsoon climate. The sites are located between two meteorological stations, Obra and Renukut. Ranitalli site is nearest to Obra and Hathinala site is nearest to Renukoot. Mean annual rainfall is 926 mm at Obra and 1146 mm at Renukoot[34]. The soils are residual ultisols, sandy loam in texture, reddish to dark grey in colour and are extremely poor in nutrients[35]. Among the four sites, the mean rainy

*For correspondence. (e-mail: hema.bhu@gmail.com)